UNIVERSITÀ DEL PIEMONTE ORIENTALE

**School of Medicine**

*Department of Translational Medicine*

**PhD Program in Science and Medical Biotechnology**

**XXXIV CYCLE**

# LIQUID BIOPSY PROVIDES COMPLEMENTARY INFORMATION TO TISSUE BIOPSIES FOR MOLECULAR CLASSIFICATION OF DLBCL PATIENTS

TUTOR:

**Chiar.mo Prof. Gianluca GAIDANO**

Coordinator:

**Prof. Marisa GARIGLIO**

Candidate: **Sruthi SAGIRAJU**

Matricula: **20022310**

Academic Year 2020/2021

# INDEX

# ABSTRACT

Diffuse large B-cell lymphoma (DLBCL) is a molecular heterogeneous disease and patients have a variable clinical course and prognosis. GEP has identified 3 molecular subtypes according to COO: germinal center B-cell-like (GCB)-DLBCL, activated B-cell-like (ABC)-DLBCL and unclassified cases. Recent genomic studies have identified different molecular clusters on tissue biopsy samples harboring unique genetic lesions and therapeutic vulnerabilities. However, different anatomical sites of the disease may harbor unique genetic lesions that are not captured in the diagnostic tissue biopsy. In this contest, liquid biopsy is a non-invasive tool that allows the collection of circulating tumor DNA (ctDNA) shed by apoptotic tumor cells potentially deriving from all the different sites of the lymphoma. This may provide an integrative source of tumor DNA for DLBCL genotyping, for clonal evolution assessment, and for the identification of genetic mechanisms of resistance.

The aims of the study are: *i)* to identify new prognostic molecular markers on ctDNA and on lymph node biopsy; and *ii*) to compare the DLBCL molecular clusters between the lymph node biopsy (LN) and the ctDNA in newly diagnosed DLBCL patients.

The mutational profiling performed in 77 DLBCL patients treated with R-CHOP, through a NGS approach, allows to identify at least one somatic non-synonymous mutation in 92.2% (71/77) of patients in the LN biopsy, and in 87.0% (67/77) in the ctDNA. Mutation analysis of different compartments allowed to identify mutations with potential clinical impact. In particular, *GRHPR* ($p$=0.035) and *SGK1* ($p$=0.039) mutations identified only on the liquid biopsy, and *MYC* mutations identified only on the lymph node biopsy ($p$=0.021) were associated with a shorter PFS. Moreover, ctDNA levels harbor prognostic impact since higher levels of ctDNA (≥2.5 log hGE/mL) showed a significantly worse PFS ($p$=0.025) and OS ($p$=0.004). Based on the mutational landscape identified, the LymphGen tool allowed to assign to a specific molecular cluster 46.5% (33/71) of patients on the LN biopsy, and 40.3% (27/67) on the liquid biopsy. The combination of mutational data from LN and ctDNA improved DLBCL assignment to a specific cluster, thus classifying 48.7% (36/74) of cases. From a clinical perspective, by combining mutational data from the LN and from the ctDNA, patients belonging to the BN2 and ST2 clusters showed a favorable outcome with a 36-month PFS of 100% compared to 62.3% for patients belonging to the MCD or EZB clusters ($p$ = 0.040). The combination of mutational data from LN biopsy and liquid biopsy provides complementary information for the molecular classification and prognostic stratification of newly diagnosed DLBCL patients.

# 1. INTRODUCTION

## 1.1 Diffuse large B-cell lymphoma (DLBCL)

Diffuse large B cell lymphoma (DLBCL) is the most common lymphoid malignancy in adults with an annual incidence of over 100.000 cases worldwide, accounting for up to 35% of non-Hodgkin lymphomas (NHL) (Teras *et al.*, 2016). DLBCL is a highly heterogeneous group of neoplasms and patients have a variable clinical course and prognosis (Li *et al.*, 2018). Approximately 50-60% of DLBCL patients are cured with the rituximab plus cyclophosphamide, doxorubicin, vincristine, and prednisone (R-CHOP) treatment, however, the majority of the DLBCL patients remain incurable (relapsed/refractory patients; R/R) and die due to progressive disease (Tilly *et al.*, 2015; Zhang *et al.*, 2015).

Novel molecular studies have characterized the pathogenesis of DLBCL and identified molecular subgroups of patients with different clinical outcome and for whom different therapeutic strategies should be applied. DLBCL results from the malignant transformation of mature B cells that have experienced the germinal center (GC) reaction (Pasqualucci *et al.*, 2018). GCs are dynamic compartments that form when B cells are challenged by a foreign antigen and represent the primary site for clonal expansion and antibody affinity maturation (De Silva *et al.*, 2015; Mesin *et al.*, 2016). Gene expression profile analysis has identified two major subtypes of DLBCL according to cell of origin (COO): *i)* germinal center B-cell-like (GCB) DLBCL, which derives from GC light zone B cells, and *ii)* activated B-cell-like (ABC) DLBCL, which originates from a later stage of GC differentiation when B cells are committed to plasmablastic differentiation (Alizadeh *et al*., 2000) (Figure 1).

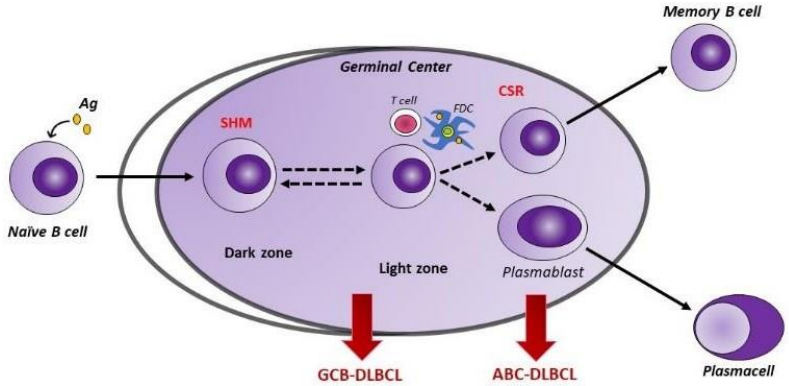


**Figure 1. Cell of origin of DLBCL subtypes**

In addition, 15-30% of cases remain unclassified and represent a unique entity with peculiar molecular and clinical features (Alizadeh *et al*., 2000). Consistent with their putative COO, GCB-DLBCLs display high-level expression of the master regulator B-cell lymphoma/leukemia-6 (BCL-6) and harbour hypermutated immunoglobulin (Ig) genes with ongoing somatic hypermutation, whereas ABC-DLBCLs show activation of nuclear factor kappa-light-chain-enhancer of activated B cells (NF-κB) and B-cell receptor (BCR) signaling pathways and upregulation of genes required for plasmatic differentiation (Shaffer *et al.*, 2012). DLBCL risk stratification according to COO has prognostic value upon R-CHOP treatment. GCB-DLBCL patients have a more favourable clinical outcome, whereas ABC-DLBCL patients fail more frequently this kind of immunochemotherapy (Rosenwald *et al.*, 2002; Thieblemont *et al.*, 2011; Scott *et al.*, 2015; Dunleavy *et al.*, 2014) (Figure 2).

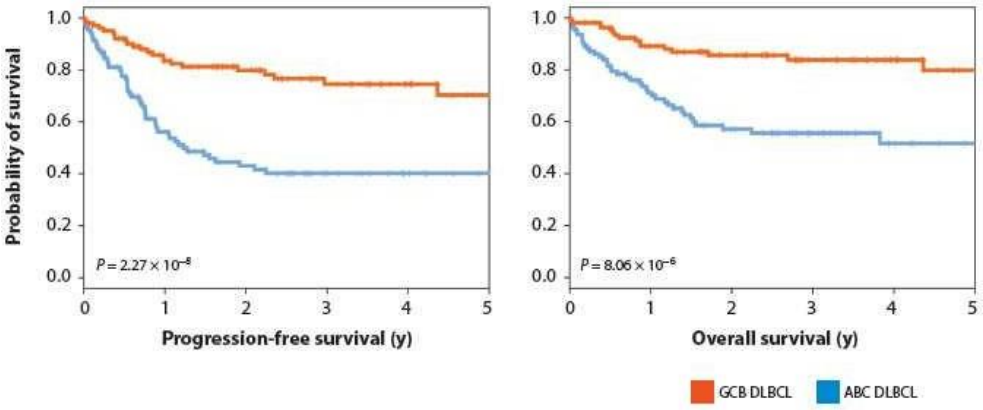


**Figure 2. Outcome of GCB-DLBCL and ABC-DLBCL with R-CHOP**

## 1.2 Molecular pathogenesis of DLBCL

DLBCL pathogenesis is associated with a consistent number of genetic lesions; some of them are shared in both GCB and ABC-DLBCL, whereas others are unique of each molecular subtype. Genetic lesions found in both GCB and ABC-DLBCL include: *i)* alterations of histone/chromatin modifiers; *ii)* deregulation of BCL-6 activity; *iii)* escape from immune surveillance, and *iv)* other mutations including somatic copy number alterations (SCNAs) and structural variants (SVs).

***i)* Alterations of histone/chromatin modifiers:**

Monoallelic and biallelic somatic mutations of lysine-specific methyltransferase 2D (*KMT2D*) gene are found in 30% of DLBCL cases, representing the single most frequent genetic aberration associated with this disease (Morin *et al.,* 2011; Pasqualucci *et al.,* 2011). The *KMT2D* gene encodes a member of the SET1 family of histone methyltransferases that induce an active chromatin conformation by predominantly trimethylating the lysine at position 4 of histone H3 (H3K4) (Shilatifard *et al.,* 2012). *KMT2D* mutations comprise mostly truncating events and missense mutations that impair the protein enzymatic function by removing the C-terminal cluster of conserved domains, including the SET domain (Morin *et al.,* 2011; Pasqualucci *et al.,* 2011). Deletion of *KMT2D* in mouse pre-GC B cells leads to a significant expansion of GC B cells, supporting the notion that *KMT2D* inactivation is an early event (Zhang *et al.,* 2015).

One-third of DLBCL samples displays somatic mutations and/or deletions affecting the acetyltransferase genes coding for CREB binding protein (*CREBBP*) (∼50% in GCB-DLBC and ∼30% in ABC-DLBCL) and, less frequently, the E1A binding protein P300 (*EP300*) (Pasqualucci *et al.,* 2011). These enzymes are pleiotropic regulators of gene expression that catalyze the addition of acetyl groups to specific lysine residues in histone and non-histone proteins, also including tumor protein p53 (TP53) (Brooks*et al.,* 2011; Goodman *et al.,* 2000). DLBCL-associated mutations and small insertion or deletion (indels) disrupt the function of the CREBBP/EP300 proteins either by removing the histone acetyltransferase domain or by introducing amino acid changes within this domain, which cause diminished affinity for Acetyl-CoA (Pasqualucci *et al.,* 2011).

***ii)* Deregulation of BCL-6 activity:**

Approximately one-third of DLBCL cases carries chromosomal translocations that prevent *BCL-6* downregulation by positioning the intact coding domain of the gene downstream to heterologous promoter sequences derived from chromosomal partners, leading to deregulationof *BCL-6* expression by a mechanism known as “promoter substitution” (Iqbal *et al.,* 2007; Ye*et al.,* 1995). As a consequence, chromosomal translocations induce constitutive *BCL-6* expression and pathologic maintenance of GC phenotype, including tolerance to DNA damage and block of terminal differentiation (Pasqualucci *et al.,* 2018). The *BCL-6* gene can be also altered by somatically acquired point mutations and some abrogate a negative autoregulatory loop by which the BCL-6 protein controls its own transcription (Pasqualucci *et al.,*1998; Shen *et al.,*1998; Pasqualucci *et al.,* 2003; Wang *et al.,* 2002).

In addition to alterations that directly involve the *BCL-6* locus, several other genetic lesions deregulate the expression of *BCL-6* by alternative or indirect mechanisms. Deleterious mutations of *CREBBP/EP300* impair acetylation-mediated inactivation of the BCL-6 transrepressive function (Pasqualucci *et al.,* 2011; Bereshchenko *et al.,* 2002). Approximately 15% of cases display somatic mutations in the myocyte enhancer binding factor 2B (*MEF2B*) (Morin *et al.,* 2011; Ying *et al.,* 2013). *MEF2B* mutations enhance its transactivator function and consequently *BCL-6* expression (Ying *et al.,* 2013). Lastly, 5% of DLBCL cases display loss-of-function mutations and/or deletions of F-box only protein 11 (*FBXO11*), a ubiquitin adaptor protein that normally targets BCL-6 for proteasomal degradation (Duan *et al.,* 2012; Schneider *et al.,* 2016).

***iii)* Escape from immune surveillance:**

Approximately 60% of DLBCL samples fail to express the major histocompatibility complex (MHC) class I due to a variety of genetic and epigenetic mechanisms. These include: *i)* deletions of the *B2M* locus, encoding for the beta-2-microglobulin variant subunit which is necessary for the formation of human leukocyte antigen class I (HLA-I) complex on the cell surface; *ii)* point mutations; and *iii)* genomic loss of the *HLA* loci and lack of expression or aberrant cytoplasmic localization of the B2M/HLA-I protein represent the genetic and epigenetic mechanisms of immune evasion (Challa-Malladi *et al.,* 2011).

***iv)* Other lesions:**

*TP53* mutations are present in about 20% of DLBCL cases and have been shown to be an independent predictor of poorer prognosis (Karube *et al.,* 2018; Young *et al.,* 2007; Ichikawa *et al.,* 1997; Kerbauy *et al.,* 2004; Xu-Monette *et al.,* 2012). Mutations in *TP53* usually result in loss-of-function and can occur in the DNA binding domain or in other locations; DNA binding domain mutations have greater adverse prognostic impact (Karube *et al.,* 2018; Young *et al.,* 2007; Xu-Monette *et al.,* 2012). Forkhead box protein O1 (*FOXO1*) mutations were identified in 8% to 10% of all DLBCL cases. These mutations, localized in the first exon, particularly in the N-terminal region, in the DNA binding domain and comprise amino acid changes that cluster around a phosphorylation site required for serine/threonine kinase (AKT)-mediated nuclear-cytoplasmic translocation, likely preventing the inactivation of FOXO1 in response to phosphoinositide 3-kinase (PI3K) signaling (Trinh *et al.,* 2013). The transcription factor FOXO1 is a key player during B cell differentiation, and its activity is negatively regulated by PI3K-AKT (Dominguez-Sola *et al.,* 2015). As consequence, alterations within

*FOXO1* decrease OS in patients treated with R-CHOP (Trinh *et al.,* 2013).

## 1.3 Genetic lesions associated with GCB-DLBCL

The genetic lesions that have been associated preferentially with GCB-DLBCL include: *i)* chromosomal translocations of B-cell lymphoma/leukemia-2 (*BCL-2*) and myelocytomatosis viral oncogene homolog (*MYC*) genes; *ii)* mutations of the enhancer of zeste homolog 2 (*EZH2*) methyltransferase; *iii)* mutations of the tumor necrosis factor-receptor superfamily member 14 (*TNFRSF14*) and *iv)* alterations affecting B cell migration.

***i)* Chromosomal translocations of *BCL-2* and *MYC*:**

*BCL*-2 is a key antiapoptotic molecule expressed in most tissues but absent in the GC, consistent with the need of GC B cells to maintain a default proapoptotic program (Saito *et al.*, 2009; Iqbal *et al.*, 2004). In ~30% of GCB-DLBCL, the t(14;18) translocation juxtaposes the *BCL-2* coding exons under the control of the immunoglobulin (IG) locus, resulting in its constitutive expression. Deregulation of BCL-2 has been associated with an inferior outcome, particularly coupled with *MYC* deregulation (Barrans *et al.*, 2003).

The *MYC* gene encodes for a transcription factor that controls numerous biological functions, including proliferation, cell growth, telomerase activity, energy metabolism, differentiation, and apoptosis (Conacci-Sorrell *et al.*, 2014). *MYC* is ectopically and constitutively expressed in 10% to 14% of GCB- DLBCLs, often as the result of chromosomal translocations that join its intact coding domain to the IG heavy or light chains loci (Karube *et al.*, 2015; Dalla-Favera *et al.*, 2010). The presence of *MYC* translocations has been linked to worse prognosis in DLBCL (Barrans *et al.*,2010). In 5% to 10% of DLBCL, chromosomal translocations of *MYC* and *BCL-2* coexist (Burotto *et al.*, 2016).

In the latest World Health Organization (WHO) Classification was introduced a new entity, termed high-grade B cell lymphoma (HGBL), characterized by the presence of *MYC* and *BCL2* and/or *BCL6* rearrangements, DLBCL morphology and with worst outcome when treated with R-CHOP chemotherapy. As consequences, more intensive chemotherapy is required, R-EPOCH (rituximab, etoposide phosphate, prednisone, vincristine sulfate, cyclophosphamide, and doxorubicin hydrochloride) in an effort to improve outcome (Barrans *et al.*, 2010).

***ii)* Mutations of *EZH2* methyltransferase:**

*EZH2* encodes a SET-domain histone methyltransferase that is responsible for trimethylating the lysine 27 residue of histone H3 (H3K27me3) (Czermin *et al.,* 2002). Approximately 22% of GCB-DLBCL display heterozygous *EZH2* gene mutations, which in most cases replace a single evolutionarily conserved residue (Y641) within the protein SET domain, enhancing its ability to catalyze the addition of H3K27me3 mark (Morin *et al.*, 2010; Sneeringer *et al.*, 2010).

***iii)* Mutations of *TNFRSF14*:**

*TNFRSF14* encodes for a member of the tumor necrosis factor-receptor superfamily that is expressed in both T and B cells and can deliver opposing signals based on its specificity for diverse ligands (Steinberg *et al*., 2011). High TNFRSF14 expression correlates with poor overall survival (OS) and progression-free survival (PFS) (Carreras *et al*., 2019). Deletions and mutations of *TNFRSF14*, including missense (~50%), nonsense (~40%), and frameshift (2.5%) events confined to the exons encoding for its ectodomain, are recurrently found in DLBCL and segregate with the GCB subtype (30% of cases) (Boice *et al*., 2016). One mechanism underlying the tumorigenic effect of *TNFRSF14* loss is the inhibition of cell-cell interactions between this receptor and its ligand B- and T-lymphocyte attenuator (BTLA), which induces a tumor-supportive microenvironment (Boice *et al*., 2016).

***iv)* Alterations affecting B cell migration:**

The GC, specialized microstructure in the secondary lymphoid tissues, physiologically produces plasma cells (PCs) secreting antibodies and memory B cells upon infection or immunization (Stebegg *et al.,* 2018). The confinement of B cells within this microenvironment is modulated by the activity of two GC-specific-G-protein–coupled receptors (GPCRs): sphingosine-1-phosphate receptor 2 (S1PR2) and the orphan purinergic receptor P2RY8. In response to lipid ligands, these receptors recruit two closely related G proteins (Ga12 and Ga13) (McCabe *et al*., 2012; Green *et al*., 2012).

Within the GC, B cells undergo somatic mutations of the gene, encoding their receptors, which can lead to B cell clones to bind antigen with high affinity (Stebegg *et al*., 2018). However, this mutation can also have negative effects, as it can be involved in multiple inflammatory states, including autoimmune disease and cancer (Pitzalis *et al*., 2014).

In particular, Green *et al*., described recurrent inactivating mutations in several components of the above, mentioned pathway, in the GCB-DLBCL subtype (Green *et al.*,

2012). Accordingly, disruption of the GC architecture, eventually leads the spread of malignant GC B cells to the peripheral blood (PB) and bone marrow (BM). (Muppidi *et al.,* 2014; Cattoretti *et al.,* 2009).

## 1.4 Genetic lesions associated with ABC-DLBCL

The core biology of ABC-DLBCL is defined by alterations leading to constitutive activation of NF-κB pathway, the expression of which is required for ABC-DLBCL survival (Pasqualucci *et al.,* 2018). These lesions include: *i)* mutations in the B cell receptor (BCR) signaling pathway; *ii)* mutations of myeloid differentiation primary response 88 (*MYD88*); *iii)* mutations of tumor necrosis factor alpha-induced protein 3 (*TNFAIP3*); and *iv)* lesions blocking terminal B cell differentiation.

***i)* Mutations in the BCR signaling pathway:**

ABC-DLBCL displays a "chronic active" form of BCR signaling that is sustained by genetic alterations affecting proximal members of the pathway (Davis *et al.,* 2010). In 21% of cases, these are gain-of-function mutations in the immunoreceptor tyrosine-based activation motifs of cluster of differentiation 79B *(CD79B*), which maintain BCR signaling by attenuating a negative feedback (Davis *et al.,* 2010). In 9% of cases, mutations involve the gene encoding the caspase recruitment domain family member 11 *(CARD11*) (Lenz *et al.,* 2008), a component of the "signalosome" complex that needs to be assembled for the proper transduction of BCR signaling (Thome *et al.,* 2004). These events cluster in the exons encoding for the protein coiled-coil domain and enhance the ability of *CARD11* to transactivate NF-κB target genes (Davis *et al.,* 2010; Knies *et al.,* 2015).

***ii)* Mutations of *MYD88*:**

Approximately 30% of ABC-DLBCLs harbour mutations leading to a hotspot L265P substitution in the hydrophobic core of the MYD88 Toll/interleukin-1 receptor (TIR)-domain. This adaptor molecule is critical for relaying signals from the TLR to NF-κB transcription complex (Ngo *et al.,* 2011; Lam *et al.,* 2008). In particular, L265P substitution induces interleukin-1 receptor-associated kinase 4 (IRAK4) activity and phosphorylation through the spontaneous assembly of a protein complex containing interleukin 1 receptor-associated kinase 1 (IRAK1) and IRAK4, which in turn can activate NF-κB and the Janus kinase/signal transducers and activators of transcription (JAK/STAT3) responses (Rhyasen *et al.,* 2015).

***iii)* Mutations of *TNFAIP3*:**

Nearly 30% of ABC-DLBCL cases display biallelic truncating mutations and/or focal deletions inactivating the *TNFAIP3* gene, which encodes a dual function ubiquitin-modification enzyme involved in the negative regulation of NF-κB responses triggered by TLR and BCR signaling (Compagno *et al.,* 2009; Kato *et al.,* 2009; Boone *et al.,* 2004). Inactivationof TNFAIP3/A20 may thus contribute to lymphomagenesis by reducing inappropriately prolonged NF-κB responses (Compagno *et al.,* 2009; Kato *et al.,* 2009).

***iv)* Lesions blocking terminal B cell differentiation:**

In ABC-DLBCL, genetic driven constitutive activation of NF-κB, is frequently complemented by lesions, blocking terminal B cell differentiation. 25% of cases displays biallelic loss of function mutations/deletions of PR domain-containing protein 1 Positive regulatory domain factor 1 (PRDM1)/β-interferon gene positive regulatory domain I-binding factor (BLIMP1), a transcriptional repressor committed to plasmacytic differentiation and required for PCs development (Pasqualucci *et al.,* 2018).

## 1.5 Novel DLBCL molecular subtypes

The advent of gene expression profile (GEP), which was used to define two prominent COO subtypes, GCB-DLBCL and ABC-DLBCL, and a third subtype, consisting of "unclassified" cases, started the initial progress toward a molecular diagnosis of DLBCL subtypes (Alizadeh *et al.,* 2000; Rosenwald *et al.,* 2002). This classification has proved useful in understanding the different responses of DLBCL patients to target therapies (Wilson *et al.,* 2015). However, the COO distinction, providing a phenotypic rather than genetic description, does not fully account for the different outcomes, following chemotherapy and targeted therapy (Wright *et al.,* 2020). Several studies have recently identified genetic subtypes, characterized by distinct outcomes and pathway dependencies (Chapuy *et al.,* 2018; Schmitz *et al.,* 2018; Wright *et al.,* 2020).

In their study, Chapuy and colleagues conducted a comprehensive genetic analysis of 304 primary DLBCLs. By integrating recurrent mutations, low-frequency alterations, SCNAs and SVs identified, they defined five DLBCL subsets and one small subset of 12 DLBCLs (termed cluster 0), with different prognostic significance, in terms of both PFS and OS. **Cluster 1 (C1):** favorable outcome ABC-DLBCLs with extrafollicular genetic features, possibly marginal zone (MZ) origin. C1 DLBCLs exhibited BCL6 SVs in combination with aberrations

of notch receptor 2 (*NOTCH2*) signaling pathway components and mutations affecting different components of the NF-κB pathway members: BCL10 immune signaling adaptor (*BCL10*), *TNFAIP3* and Fas cell surface death receptor (*FAS*). **Cluster 3 (C3):** poor risk GCB-DLBCLs with BCL2 SVs and alterations of phosphatase and tensin homolog (*PTEN*), *KMT2D*, *CREBBP*, *EZH2*, hydrogen voltage gated channel 1 (*HVCN1*) and G protein subunit alpha 13 (*GNA13*), B cell transcription factors myocyte enhancer factor 2B (*MEF2B*), interferon regulatory factor 8 (*IRF8*), BCR signaling, PI3K signaling and in TNFSF14 pathway. **Cluster 4 (C4):** newly defined group of good-risk GCB-DLBCLs with distinct alterations in BCR/PI3K, JAK/STAT, and BRAF pathway components and intermediates Ras homolog family member A (*RHOA*), *GNA13*, and serum/glucocorticoid regulated kinase 1 (*SGK1*), NF-κB modifiers, NF-κB inhibitor ε (*NFKBIE*), NF-κB inhibitor α (*NFKBIA*), and *STAT3*. **Cluster 2 (C2):** COO-independent group of tumors with biallelic inactivation of *TP53* and 17p, 9p21.3/CDKN2A and 13q14.2/retinoblastoma-associated protein (*RB1*) copy loss, which perturb chromosomal stability and cell cycle. **Cluster 5 (C5):** less favorable outcome ABC-DLBCLs, characterized by 18q gain, increasing the expression of driver genes, such as *BCL2* and mucosa-associated lymphoid tissue lymphoma translocation protein 1 (*MALT1*) (Ennishi *et al.,* 2017; Dierlamm *et al.,* 2008), *CD79B* and *MYD88* aberrations (Ngo *et al.,* 2011; Davis *et al.,* 2010; Dubois *et al.,* 2017). **Cluster 0 (C0):** small subset of 12 DLBCLs, lacking genetic drivers, with good outcome. This group includes a morphologically defined subtype of T cell/histocyte-rich large B DLBCS (THRLBC), characterized by inflammatory/immune cell infiltration (Chapuy *et al.,* 2018).

In the same year, Schmitz *et al*. studied ~500 DLBCLs, using exome and transcriptome sequencing, array-based DNA CN analysis and targeted amplicon resequencing of 372 genes to identify more recurrent aberrant genes and pathways (Schmitz *et al.,* 2018). They classified four genetic DLBCL subtypes, applying a predictor algorithm, termed Genclass (based on mutations in 50 genes and translocations of *BCL2* and *BCL6*): *i)* **MCD** subtype, characterized by a less favorable outcome ABC-DLBCLs with the co-occurrence of *MYD88* L265P and *CD79B* mutations. MCD subtype has frequent gain or amplification of *SPIB*, encoding a transcription factor that, with interferon regulatory factor 4 (*IRF4*), defines and promotes the plasmacytic differentiation; *ii)* **BN2** subtype, characterized by good response to immunochemotherapy. This cluster exhibits *BCL6* fusions and *NOTCH2* mutations or amplification, spen family transcriptional repressor (*SPEN*) mutations as well as mutations in Deltex E3 Ubiquitin Ligase 1 (*DTX1*). The NF-κB pathway and BCR-dependent NF-κB pathway aberrations are prominent features of BN2 subtype, in details alterations in *TNFAIP3*,

TNFAIP3 interacting protein 1 (*TNIP1*), protein kinase C β (*PRKCB*); *iii)* **N1** subtype, dominated by ABC-DLBCL cases and characterized by inferior outcomes, harbours notch receptor 1 (*NOTCH1*) mutations and aberrations targeting *IRF4*, transcriptional regulators of B cell differentiation, inhibitor of DNA binding 3 (*ID3*) and BCL6 corepressor (*BCOR*), which may contribute to its plasmocytic phenotype; *iv)* **EZB** subtype, a favorable outcome GCB-DLBCL subtype, is based on *BCL2* translocations, *EZH2* mutations, and NF-κB proto-oncogene subunit (REL) amplification, as well as aberrations of the tumor suppressor genes (*TNFRSF14*, CREBBP, *EP300*) (Schmitz *et al.,* 2018). Unclassified cases are enriched for aberrations targeting *SPEN* and *NOTCH1*; *NOTCH2* mutations and *BCL6* fusions significantly co-occurred and distinguished these DLBCLs from others (Schmitz *et al.,* 2018).

In a later study, Wright *et al.* created an algorithm, termed LymphGen to provide probabilistic classification of individual DLBCL patient into genetic subtypes, based on the presence or absence of predictor genes aberrations (i.e., mutations, copy number variations (CNVs) or fusions).

LymphGen defines subtype predictor features expanding to seven the number of DLBCLs subtypes, defined in their study by Schmitz *et al.*, (Schmitz *et al.,* 2018): MCD (including *MYD88* L265P and *CD79B* mutations); BN2 (including *BCL6* translocations and *NOTCH2* mutations); N1 (including *NOTCH1* mutations); and EZB (including *EZH2* mutations and *BCL2* translocations) (Schmitz *et al.,* 2018; Wright *et al.,* 2020). The remaining cases lead to create two new subtypes: A53, characterized by aneuploidy with *TP53* inactivation (the most frequently mutated gene (25.2%) (Chapuy *et al.,* 2018; Monti *et al.,* 2012); and ST2, associated with *SGK1* and tet methylcytosine dioxygenase 2 (*TET2*) mutations. The samples classified as "Other" had either both a *TP53* mutation and a single-copy *TP53* loss or a homozygous *TP53* deletion (Schmitz *et al.,* 2018).

## 1.6 DLBCL genotyping on the liquid biopsy

Limitations in accessing fresh tumor material from DLBCL tissue biopsies have prevented the rapid translation of DLBCL gene mutations into prognostic or predictive tools for clinical practice (Rossi *et al.,* 2017). Also, serial sampling of tumors to track the acquisition of drug-resistance mutations requires a re-biopsy of the DLBCL, which may not be routinely feasible in clinical practice (Rossi *et al.,* 2017). Therefore, alternative accessible sources of tumor DNA may help to complement the molecular diagnostic analyses that are routinely carried out on formalin-fixed paraffine-embedded (FFPE) tissue biopsies (Rossi *et al.,* 2017). The availability of tumor-specific DNA simply in plasma, serum, or other body fluids, without

the necessity of an invasive tumor biopsy, led to the concept of "liquid biopsy" in lymphoma types lacking leukemic involvement (Spina *et al.,* 2019).

Cell-free fragments of DNA (cfDNA) are shed into the bloodstream by tumor cells undergoing apoptosis and circulate in plasma as double-stranded DNA fragments that are predominantly short (<200 bp), and normally at low concentration (Fleischhacker *et al.,* 2007). Accessing tumor cfDNA through the bloodstream has clear sampling advantages and allows serial monitoring of disease genetics in real time. cfDNA is also representative of the entire tumor heterogeneity, thus enabling to bypass the anatomical biases imposed by tissue biopsies in the reconstruction of the entire cancer clonal architecture and to identify resistant clones that are dormant in non-accessible tumor sites (Jahr *et al.,* 2001). Levels of cfDNA vary across different lymphoma subtypes and the concentration of cfDNA in patients with untreated DLBCL is significantly higher than in healthy controls (26.9 ng/ml and 12.1 ng/ml respectively) (Hohaus *et al.,* 2009).

Quantification of circulating DNA by real-time PCR at diagnosis can identify patients with elevated levels that are associated with disease characteristics indicating aggressive disease and poor prognosis (Hohaus *et al.,* 2009). In DLBCL, cfDNA has been quantified or used to track tumor clonotypic immunoglobulin gene rearrangement for minimal residual disease (MRD) monitoring (Hohaus *et al.,* 2009; Kurtz *et al.,* 2015; Roschewski *et al.,* 2015; Roschewski *et al.,* 2016). During surveillance time points before relapse, high-throughput sequencing of immunoglobulin genes (Ig-HTS) from plasma circulating tumor DNA (ctDNA) demonstrated improved specificity and similar sensitivity compared with positron emission tomography combined with computed tomography (PET/CT) (Kurtz *et al.,* 2015). Given its high specificity, Ig-HTS from plasma has potential clinical utility for surveillance after complete remission (Kurtz *et al.,* 2015).

By applying a training validation approach, it has been shown that plasma cfDNA genotyping: *i)* is as accurate as genotyping of the diagnostic biopsy to detect somatic mutations of allelic abundance >20% in DLBCL; *ii)* allows the identification of mutations that are undetectable in the biopsy tissue conceivably because they are restricted to clones that are anatomically distant from the biopsy site; and *iii)* is a real-time, non-invasive tool to track clonal evolution and the emergence of treatment-resistant clones (Rossi *et al.,* 2017).

Plasma cfDNA represents a complementary source of tumor DNA for DLBCL genotyping compared with the tissue biopsy. On the one hand, the complete molecular heterogeneity of a tumor cannot be adequately assessed by a single or even multiple tissue biopsies, whereas cfDNA genotyping captures genetic information shed from all sites of the

disease. On the other hand, plasma cfDNA genotyping misses a proportion of small subclonal mutations (Rossi *et al.,* 2017). These notions suggest that liquid biopsy is not a substitute for the tumor biopsy, but instead provides complementary information in DLBCL (Rossi *et al.,* 2017).

## 1.7 DLBCL diagnosis, treatment, and prognostic factors

DLBCL is diagnosed from an excisional biopsy of a suspicious lymph node (LN), which shows sheets of large cells that disrupt the underlying structural integrity of the follicle center and stain positive for pan B cell antigens, such as CD20 and CD79A. COO is determined by immunohistochemical (IHC) stains (Liu *et al.,* 2019).

The standard therapy for patients with DLBCL is R-CHOP. Rituximab is an antibody directed against the CD20 protein, which is primarily found on the surface of B cells and is present on many lymphoma cells, while cyclophosphamide, doxorubicin, vincristine, and prednisone are chemotherapy agents (Kwak *et al.,* 2012; Chiappella *et al.,* 2013).

Using this regimen, approximately 60-70% of patients with DLBCL are cured of disease. However, about 30-40% of patients will relapse or, in a small patient's subset, be refractory to R-CHOP therapy (Li *et al.,* 2018). R-CHOP failures are principally due to either primary refractoriness or relapse after reaching a complete response (CR) (Coiffier *et al.,* 2016). Relapsed DLBCL is characterized by the appearance of any new lesion after a CR, while refractory DLBCL is defined as the failure of <50% of lesions to be reduced in size following initial treatment, as per the criteria defined by Cheson *et al.,* 2007.

*MYD88* mutation constitutively activates MYD88 signaling, which in turn activates the alternative NF-κB pathway, bypasses the BCR-dependent NF-κB activation, and confers resistance to ibrutinib (Wilson *et al.,* 2015). However, *MYD88* mutation together with *CD79A* or *CD79B* mutation, confers tumor sensitivity to ibrutinib (Wilson *et al.,* 2015). Conversely, mutations in *CARD11* or NF-κB signaling components result in the constitutive activation of the NF-κB signaling pathway independent of the upstream BCR signaling pathway, conferring potential resistance to BCR inhibitors (Wilson *et al.,* 2012).

*MYC* is rearranged in 5-15% of DLBCL patients and is frequently associated with *BCL-2* translocation, or to a lesser extent, *BCL-6* translocation, in the so-called "double hit" (i.e. rearrangements of *MYC* with either *BCL-2* or *BCL-6*) or "triple hit" (i.e. rearrangements of *MYC* with *BCL-2* and *BCL-6)* lymphomas, respectively (Green *et al.,* 2012). "Double hit" or "triple hit" B cell lymphomas patients are associated with an aggressive clinical course, poor response to conventional chemotherapy (i.e. R-CHOP) and high relapse rates (Rosenthal *et al.,*

2017).

In 2019, Rushton *et al.*, collected samples from 134 relapsed or refractory (R/R) patients enrolled in three clinical trials and performed a combination of exome sequencing and target panel sequencing of lymphoma-associated genes on ctDNA extracted from plasma samples and tissue biopsies. They found that R/R patients were enriched for mutations in six genes: *TP53, KMT2D,* interleukin 4 receptor *(IL4R*), *HVCN1*, *RB1*, and membrane spanning 4-domains A1 (*MS4A1*). *TP53* mutations and *KMT2D* were already present at the time of diagnosis but their frequency increased at the time of relapse. Moreover, *TP53* and *KMT2D* at the time of diagnosis associated with a shorter survival (Rushton *et al.*, 2019). The *MS4A1* encodes the CD20, the target of rituximab, and its mutations destabilize a common transmembrane helix leading to its lower membrane expression. *MS4A1* mutations are absent at the time of diagnosis and increased at the time of relapse predisposing to a less efficacy of anti-CD20 salvage immunochemotherapy regimen (Rushton *et al.*, 2019).

# 2. AIMS OF THE STUDY

The aims of the present study are:

*i)* To genotype both on ctDNA and on lymph node biopsy patients with newly diagnosed DLBCL;

*ii)* To identify new prognostic molecular markers both on ctDNA and on lymph node biopsy;

*iii)* To compare the molecular cluster identified on ctDNA with the one identified on lymph node.

# 3. MATERIALS AND METHODS

## 3.1 Patients

A multicenter cohort of 77 patients with diagnosed DLBCL have been included in this study. All patients were provided with synchronous samples representative of different anatomical compartments, including: *i)* tumor gDNA extracted from fresh frozen LN cells or formalin-fixed paraffin-embedded (FFPE) LN biopsies; *ii)* circulating tumor DNA (ctDNA) from plasma; and *iii)* germline gDNA extracted from granulocyte for comparative purpose. The study was approved by the Ethical Committee of the Ospedale Maggiore della Carità di Novara associated with the Università del Piemonte Orientale (study number CE 120/19). All patients provided informed consent according to the legislation established in accordance with the Declaration of Helsinki, for the use of clinical data and genetic material for research purposes.

## 3.2 Separation of granulocytes from peripheral blood (PB)

Peripheral blood (PB) granulocytes were separated by Ficoll gradient density centrifugation as source of normal germline genomic DNA (gDNA). PB was diluted in 1:2 ratio with physiological solution (NaCl 0.9%) and then centrifuged at 1800 revolutions per minute (rpm) for 25 minutes in a gradient differentiation Sigma Diagnostic™ Histopaque®- 1077 Cell Separation Medium (Sigma-Aldrich, St. Louis, MO, USA) solution to obtain granulocytes and mononuclear cells (monocytes and lymphocytes).

## 3.3 Lymph node tissue processing for gDNA extraction

The separation of tumor cells from lymph nodes was performed by processing the material into a Petri dish with Roswell Park Memorial Institute (RPMI) medium (Sigma-Aldrich, St. Louis, MO, USA) and then gently scraping the tumor tissue surface to detach the cells. Subsequently, the sample was centrifuged at 1500 rpm for 10 minutes in order to separate the tumor cells for DNA extraction.

## 3.4 Extraction of tumor and normal gDNA

Tumor and normal gDNA were extracted either by using the “salting out” protocol (Miller *et al.*, 1988). Cells were lysed with Lysis Buffer (Tris-HCl 1M, pH 8.2, NaCl 5M, EDTA

0.5M), sodium dodecyl sulphate (SDS) 20% and digested with 20 mg/mL of proteinase enzyme (pronase E).

Samples were incubated at 37°C overnight in a shaking incubator. Proteins were precipitated with 6M NaCl, and subsequently discarded after centrifugation at 3200 rpm for 20 minutes. DNA was isolated by precipitation with pure ethanol and the lactescent "jellyfish" of DNA, formed as a result of the addition of ethanol, was recovered with glass loops and washed three times in 75% ethanol. The excess of ethanol was evaporated, and the DNA was dissolved with TE Buffer (Tris-HCl 1M, pH 8.2, EDTA 0.5M).

## 3.5 Extraction of tumor gDNA from formalin-fixed paraffin-embedded (FFPE)

Tumor gDNA was isolated from fresh or formalin-fixed paraffin-embedded (FFPE) diagnostic tissue biopsies containing >70% of tumor cells, as estimated by morphology and immunohistochemistry. FFPE tissues biopsies were rehydrated with tissue SDS Buffer and transferred into microTUBE Screw-Cap. The samples were processed by using M220 focused-ultrasonicator (Covaris®,Woburn, MA, USA) to dissociate the paraffin and rehydrate the tissues for 5 minutes at 20°C (20% duty factor, 75% peak incident power, 200 cycles per burst). Proteins were digested by using proteinase K for 10 seconds (20% duty factor, 75% peak incident power, 200 cycles per burst) and with the incubation at 56°C overnight. Afterwards, samples were incubated for 1 hour at 80°C for crosslink reversing and then DNA was purifiedwith column.

## 3.6 Plasma circulating tumor DNA (ctDNA) extraction

PB samples were collected in Cell-Free DNA BCT tubes and centrifuged at 800 relative centrifugal force (rcf) for10 minutes at 4°C to separate plasma from cells. Plasma was then further centrifuged at 13.000rpm for 10 minutes at 4°C to pellet and remove any remaining cells and stored at -80°C until DNA extraction.

ctDNA was extracted from 2-3 ml aliquots of plasma immediately after thawing by using Maxwell® RSC LV ccfDNA Kit Custom (Promega Corporation, Madison, WI, USA) and quantified by Quantus Fluorometer using QuantiFluor dsDNA System (Promega Corporation, Madison, WI, USA). The quality of the extracted ctDNA was assessed by 2100 Bioanalyzer Instrument (Agilent Technologies, St. Clara, CA, USA).

## 3.7 DNA quantification and fragmentation

Tumor and germline gDNA were quantified using the Quant-iT$^{TM}$ PicoGreen dsDNA Assay kit (ThermoFisher Scientific, Eugene, OR, USA). PicoGreen is a molecule that binds selectively to double helix DNA and allows to obtain a precise estimate of the amount of DNA. The fluorimetric reading was performed using the Infinite F200 fluorometer (TECAN, Männedorf, Switzerland) using the Magellan software. The fluorimetric readings were obtained at a wavelength of 485 nm in absorption and 530 nm in emission. For quantification a standard curve was prepared using a DNA of known concentration and performing serial 1:2 scalar dilutions. Quant-iT$^{TM}$ PicoGreen dsDNA Assay kit was used at the 1:200 dilutions.

Tumor and germline gDNA from tissues were sheared through sonication with M220 focused-ultrasonicator (Covaris® Woburn, MA, USA) before library construction to obtain 250/300 base-pairs (bp) fragments. The size of the fragments was checked by using the 2100 Bioanalyzer Instrument, whereas ctDNA is naturally fragmented and was used for library construction without additional fragmentation.

## 3.8 Library design for hybrid selection

A targeted resequencing gene panel, including coding exons and splice sites of 59 genes (target region: 207299bp) that are recurrently mutated in DLBCL and in other B cell malignancies, has been specifically designed for this project.

## 3.9 CAPP-seq library preparation

The gene panel was analysed in: *i*) plasma ctDNA collected at the time of diagnosis; *ii*) germline gDNA from the paired granulocytes, for comparative purposes; *iii*) tumor gDNA from the paired tissue biopsy.

The next generation sequencing (NGS) libraries were constructed using the KAPA HyperPlus Library Preparation Kit (KAPA Biosystems, Wilmington, MA, USA), and hybrid selection was performed with the custom SeqCap EZ Hyper Prep Kit Library (Roche, Basilea, Switzerland). Multiplexed libraries (n=6 samples per run) were sequenced using 300-bp paired-end runs on MiSeq sequencer (Illumina, San Diego, CA, USA).

## 3.10 Next generation sequencing

The mutational analysis in NGS was performed using the MiSeq (Illumina, San Diego, CA, USA) platform, which allows for massive high-throughput sequencing of the genomic regions of interest. The sequencing workflow involves the following phases: *i)* generation of libraries containing the regions of interest; *ii)* sequencing; and *iii)* data analysis.

***i) Generation of libraries***

The library preparation using the KAPA HyperPrep Library Preparation Kit (KAPA Biosystems, Wilmington, MA, USA), begins with end repair and A-tailing reaction, which produces end repaired, 5'-phosphoryled, 3'-A-tailed double-stranded DNA (dsDNA) fragments, followed by the adapter ligation, during which dsDNA adapters with 3'-dTMP overhangs are ligated to 3'-dA-tailed molecules.

***ii) Sequencing***

The MiSeq Illumina sequencer is based on sequencing-by-synthesis (SBS) technology, in which DNA libraries are transferred onto a solid support called flowcell, to which they are linked by special adapters. On the flowcell the libraries are amplified by a method called bridge amplification, which generates clusters of identical DNA molecules, each derived from the amplification of a single molecule.

Sequencing is based on the reversible cyclic termination method, with a by-synthesis approach, which includes three steps: the incorporation of the nucleotide, the detection of the fluorescence image and the cut.

In the first phase of the cycle, the DNA polymerase elongates a specific primer by adding a nucleotide covalently bound to a fluorophore. This presents a block on the 3'-OH of ribose which does not allow polymerization with other nucleotides. Each nucleotide base is bound to a fluorophore of a specific colour. It follows the detection step of the image that recognizes the specific emission wavelength of the fluorophore. Next, the cut removes both the fluorophore and the inhibitory group present at the 3'-OH end, allowing the beginning of a new cycle.

Libraries were sequenced by pair-end sequencing using a 300-bp paired-end cycle kit. The library pool was denatured using 0.2N NaOH. An amount of 10 to 12 pM denatured DNA was loaded into the MiSeq reagent cartridge, which also containes all the reagents necessary for the sequencing reaction.

***iii) Data analysis***

During the sequencing run, the integrated software for real-time primary analysis (RTA, Real Time Analysis, Illumina) performs image analysis and identification of the bases and assigns a qualitative score (Phred score) to each base for each cycle. Once the primary analysis is completed, the MiSeq Reporter (Illumina) software performs a secondary analysis on the data generated by the RTA through a series of procedures that include: *i)* de-multiplexing, in which the data of different samples sequenced are pulled together based on the specific sample index sequences; *ii)* FASTQ generation, which are files containing all the reads obtained from sequencing.

FASTQ sequencing reads were deduped by using the FastUniq v1.1. Then, the deduped FASTQ sequencing reads were locally aligned to the hg19 version of the human genome assembly using the BWA v.0.6.1 software with the default setting, and sorted, indexed, and assembled into a mpileup file using SAMtools v.1.

Single nucleotide variations and indels were called in tumor gDNA or ctDNA *vs* normal gDNA, with the somatic function of VarScan2. A Z-test was used to compare the variant allele frequency *vs* the mean allele frequency in unpaired normal gDNA samples to filter out variants below the base-pair resolution background frequencies across the target region. Only variants that had a significant call in Z-test were retained (Bonferroni adjusted $p \leq 6.11x10\text{-}8$).

The variants called by VarScan 2 were annotated with the SeattleSeq Annotation 138 tool (http://snp.gs.washington.edu/SeattleSeqAnnotation138) by using the default setting. Variants annotated as SNPs according to dbSNP 138 (with the exception of *TP53* variants that were manually solved and scored as SNPs according to the International Agency for Research on Cancer *TP53* database; http://p53.iarc.fr), intronic variants mapping >2 bp before the start or after the end of coding exons, and synonymous variants were then filtered out. Splice-acceptor and splice-donor variants were annotated by using the Mutalyzer 2.0.32 tool (https://mutalyzer.nl/position-converter).

Among the remaining variants, only protein truncating variants (i.e., indels, stop codons and splice site mutations), as well as missense variants not included in the dbSNP 138 and annotated as somatic in the COSMIC v85 database (https://cancer.sanger.ac.uk/cosmic), were retained. All the variants were visualized using IGV (Integrative Genomics Viewer) software.

## 3.11 Statistical analysis

Medical statistical analysis was performed using SPSS version 24.0. (Chicago, IL, USA). Primary endpoints of survival analysis were PFS and OS. PFS was evaluated from the time of treatment start to the date of progression or death, and OS was evaluated from the time of treatment start to the date of death. Time to event outcomes (PFS and OS) were estimated using the Kaplan-Meier method and compared between groups using the Log-Rank test. To evaluate the associations between molecular features, we used Chi-square test and Fisher exact test. Statistical significance was defined as p value $< 0.05$.

## 3.12 DLBCL clusters identification with distinct genetic signatures

LymphGen 1.0 tool was used to classify an individual DLBCL patient, in both LN and plasma compartments.

The tool uses any combination of mutational data, copy number (CN) and BCL2/BCL6 rearrangement data, obtained from whole genome, exome sequencing or from targeted panel resequencing and allows for any platform besides mutational data to be omitted.

For analyses in which CN data are not available, LymphGen operates in a five-subtypes mode, omitting A53, since it is defined predominantly by CN abnormalities (https://llmpp.nih.gov/lymphgen/index.php) (Wright *et al.*, 2020).

# 4. RESULTS

## 4.1 Patients characteristics

Among the 77 patients enrolled in the study, 39/77 (50.65%) were males and 38/77 (49.35%) were females, with a median age at the diagnosis of 61 (19-88) years. According to the Ann-Arbor staging system, 9/77 (11.69%) patients were in stage I, 15/77 (19.48%) patients in stage II, 16/77 (20.78%) patients in III, 37/77 (48.05%) patients in IV. The IPI score, at diagnosis, was low (0-1) for 20 (25.97%) patients, low-intermediate (2) for 16 (20.78%) patients, high-intermediate (3) for 24 (31.17%) patients, and high (4-5) for 17 (22.08%) patients.

According to COO classification identified by Han's algorithm (Hans *et al.*, 2004), 22/77 (28.57%) cases were GCB, 40/77 (51.95%) cases were non-GCB, and 15/77 (19.48%) cases were not available. The median lactate dehydrogenase (LDH) level was 482.5 U/L (121-10245) and 39/77 (50.65%) patients presented LDH values above the upper limit of normal (450 U/L), the median Ki-67 value was 86% (40%-100%) and the median B2M value was 2941 ng/ml (1052-11440) (Table 1).

| | **Characteristics** | **Number of patients (N=77)** |
|---|---|---|
| **Gender** | Male<br>Female | 39 (50.65%)<br>38 (49.35%) |
| **Age at diagnosis** | Median<br>Range | 61<br>19-88 |
| **Ann Arbor stage** | I<br>II<br>III<br>IV | 9 (11.69%)<br>15 (19.48%)<br>16 (20.78%)<br>37 (48.05%) |
| **IPI score** | Low (0-1)<br>Low-intermediate (2)<br>High-intermediate (3)<br>High (4-5) | 20 (25.97%)<br>16 (20.78%)<br>24 (31.17%)<br>17 (22.08%) |
| **COO** | GCB<br>non-GCB<br>N/A | 22 (28.57%)<br>40 (51.95%)<br>15 (19.48%) |
| **LDH** | >ULN<br>≤ULN<br>N/A | 39 (50.65%)<br>30 (38.96%)<br>8 (10.39%) |
| **KI-67** | Median | 86 (40-100) |
| **B2M** | Median concentration | 2941 ng/ml (1052-11440) |

**Table 1. Patients baseline characteristics. IPI: International Prognostic Index; COO: cell-of-origin; GCB: Germinal Center B- cell like; non-GCB: non-Germinal Center B-cell like; LDH: lactate dehydrogenase; ULN: Upper Limit Normal; B2M: β2-microglobulin.**

After a median follow-up of 27.1 months, 18/77 (23.4%) patients had disease progression and 15/77 (19.5%) died. The median PFS was 52 months, and the median OS was 62.9 months.

## 4.2 Mutational profile

Mutational analysis on tumor gDNA and ctDNA samples was performed for all 77 patients enrolled in the study. Mutations detected in tumor gDNA, in ctDNA or in both were found for 58 of the 59 genes included in the gene panel. Mutation analysis identified at least one somatic non-synonymous mutation in 92.2% (71/77) of patients in the LN biopsy, and in 87.0% (67/77) in the ctDNA. In total, 725 mutations have been identified, among which 362/725 (49.93%) mutations were shared in both compartments, 179/725 (24.69%) mutations were identified only in gDNA and 184/725 (25.38%) mutations only in ctDNA. The average number of mutations identified in each patient on tumor gDNA and on ctDNA was 7.

The most frequently mutated genes identified in tumor gDNA from the LN biopsy were: *KMT2D*, mutated in 24/77 patients (31.17%); *PIM1*, mutated in 19/77 patients (24.68%); *HIS1THIE* and *TP53* mutated in 18/77 patients (23.38%); *TNFAIP3* and *B2M* mutated in 13/77 patients (16.88%); *ACTB* and *CREBBP* mutated in 12/77 patients (15.58%); *HIST1HIC*, *MYD88* and *NFKBIE* mutated in 11/77 patients (23.38%); *GNA13* mutated in 10/77 patients (12.99%); *CARD11*, *CD58*, *FAS* and *HIST1H2AM* mutated in 9/77 patients (11.69%); *BTG1*, *CD79B*, *HIST1H2BC*, *SGK1* and *TNFRSF14* mutated in 8/77 patients (10.39%); *HIST1H1B*, *IRF8*, *NOTCH2*, , *STAT3* and *NFKBIA* mutated in 7/77 patients (9.09%); *BCL2*, *ETV6*, *EZH2*, *MYC*, *PRDM1*, *SPEN* and *ZFP36L1* mutated in 6 /77 patients (7.79%); *BCL10*, *CD70*, *CD83*, *HIST1H2BK*, *RHOA*, *TBL1XR1*, *TMEM30A* and *UBE2A* mutated 5/77 patients (6.49%); *BRAF*, *HIST1H1D*, *KLHL6* and *MEF2B* mutated in 4/77 patients (5.19%); *BCL6*, *GRHPR*, *HIST1H2AC*, and *TOX* mutated in 3/77 patients (3.90%); *SF3B1*, *BTK*, *HVCN1* and *ZC3H12A* mutated in 2/77 patients (2.60%); *CD274*, *LTB*, *PLCG2*, *PTEN* and *ZEB2* mutated in 1/77 patients (1.30%) (Figure 3A-3C-4).

The most frequently mutated genes identified in ctDNA were: *KMT2D* mutated in 26/77 patients (33.77%); *HISTH1E* and *PIM1* mutated in 21/77 patients (27.27%); *TP53* mutated in 19/77 patients (24.68%); *TNFAIP3* mutated in 14/77 patients (18.18%); *HIST1H2AM* and *MYD88* mutated in 12/77 patients (15.58%); *CREBBP* and *HIST1H1C* mutated in 11/77 patients (14.29%); *TNFRSF14* mutated in 10/77 patients (12.99%); *ACTB*, *NFKBIE* and *B2M*

mutated in 9/77 patients (11.69%); *NOTCH2*, *FAS*, *GNA13*, *SGK1*, *SPEN* and *STAT3* mutated in 8/77 patients (10.39%); *CD58*, *HIST1H1D* and *IRF8* mutated in 7/77 patients (9.09%); *BCL10*, *BTG1*, *CARD11*, *HIST1H1B*, *HIST1H2BK*, *KLHL6*, *PRDM1*, *RHOA*, *TMEM30A* and *ZFP36L1* mutated in 6/77 patients (7.79%); *BCL2*, *CD79B*, *EZH2*, *HIST1H2BC*, *MEF2B*, *NFKBIA*, *TBL1XR1* and *UBE2A* mutated in 5/77 patients (6.49%); *ETV6*, *TOX*, *ZC3H12A* and *ZEB2* mutated in 4/77 patients (5.19%); *BCL6*, *CD70*, *CD83* and *MYC* mutated in 3/77 patients (3.90%); *BRAF*, *GRHPR*, *HIST1H2AC*, *HVCN1*, *LTB* and *SF3B1* mutated in 2/77 patients (2.60%); *BTK*, *PLCG2* and *PTEN* mutated in 1/77 patients (1.30%); *CD274* was not mutated in any ctDNA sample (Figure 3B-3C-4).

A

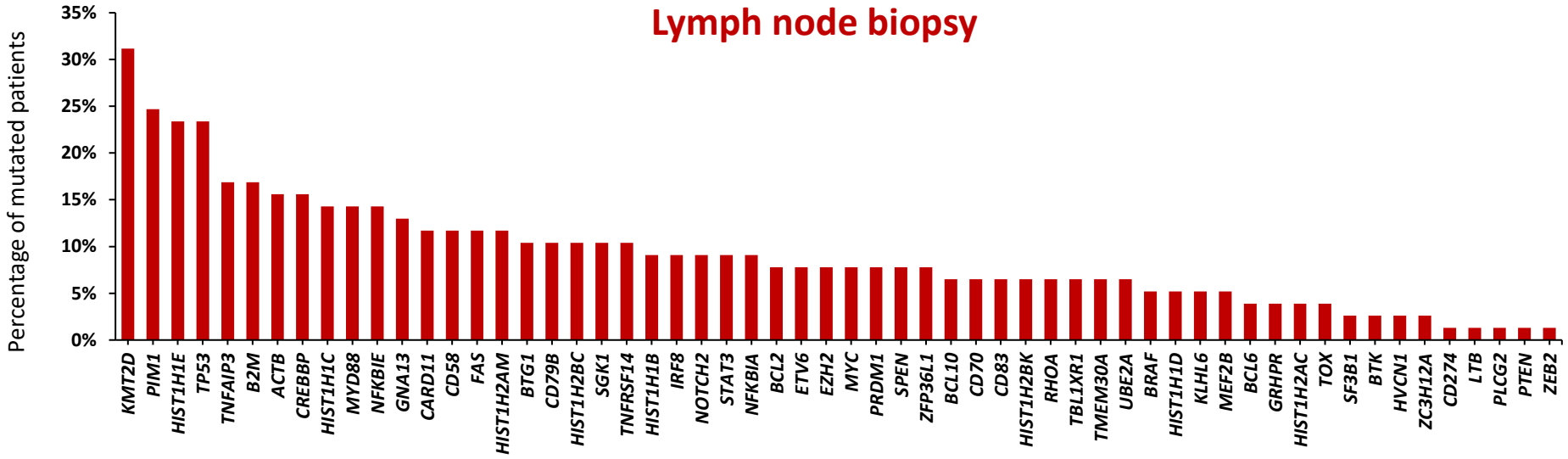
Lymph node biopsy
Percentage of mutated patients
35%
30%
25%
20%
15%
10%
5%
0%
KMT2D PIM1 HIST1H1E TP53 TNFAIP3 B2M ACTB CREBBP HIST1H1C MYD88 NFKBIE GNA13 CARD11 CD58 FAS HIST1H2AM BTG1 CD79B HIST1H2BC SGK1 TNFRSF14 HIST1H1B IRF8 NOTCH2 STAT3 NFKBIA BCL2 ETV6 EZH2 MYC PRDM1 SPEN ZFP36L1 BCL10 CD70 CD83 HIST1H2BK RHOA TBL1XR1 TMEM30A UBE2A BRAF HIST1H1D KLHL6 MEF2B BCL6 GRHPR HIST1H2AC TOX SF3B1 BTK HVCN1 ZC3H12A CD274 LTB PLCG2 PTEN ZEB2

B

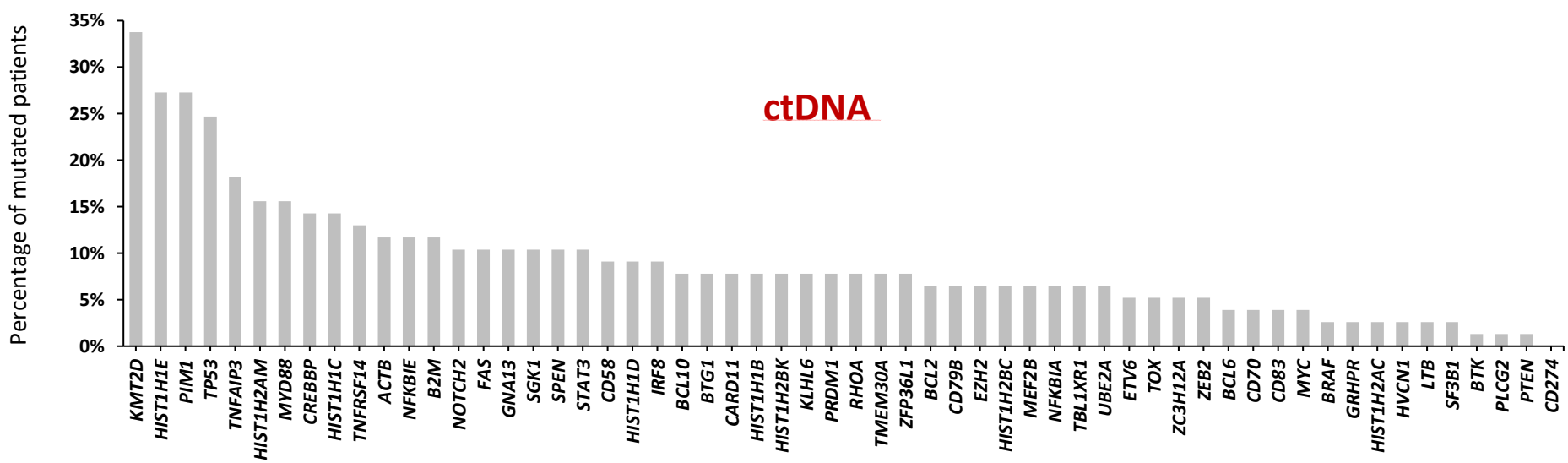
ctDNA
Percentage of mutated patients
35%
30%
25%
20%
15%
10%
5%
0%
KMT2D HIST1H1E PIM1 TP53 TNFAIP3 HIST1H2AM MYD88 CREBBP HIST1H1C TNFRSF14 ACTB NFKBIE B2M NOTCH2 FAS GNA13 SGK1 SPEN STAT3 CD58 HIST1H1D IRF8 BCL10 BTG1 CARD11 HIST1H1B HIST1H2BK KLHL6 PRDM1 RHOA TMEM30A ZFP36L1 BCL2 CD79B EZH2 HIST1H2BC MEF2B NFKBIA TBL1XR1 UBE2A ETV6 TOX ZC3H12A ZEB2 BCL6 CD70 CD83 MYC BRAF GRHPR HIST1H2AC HVCN1 LTB SF3B1 BTK PLCG2 PTEN CD274

C

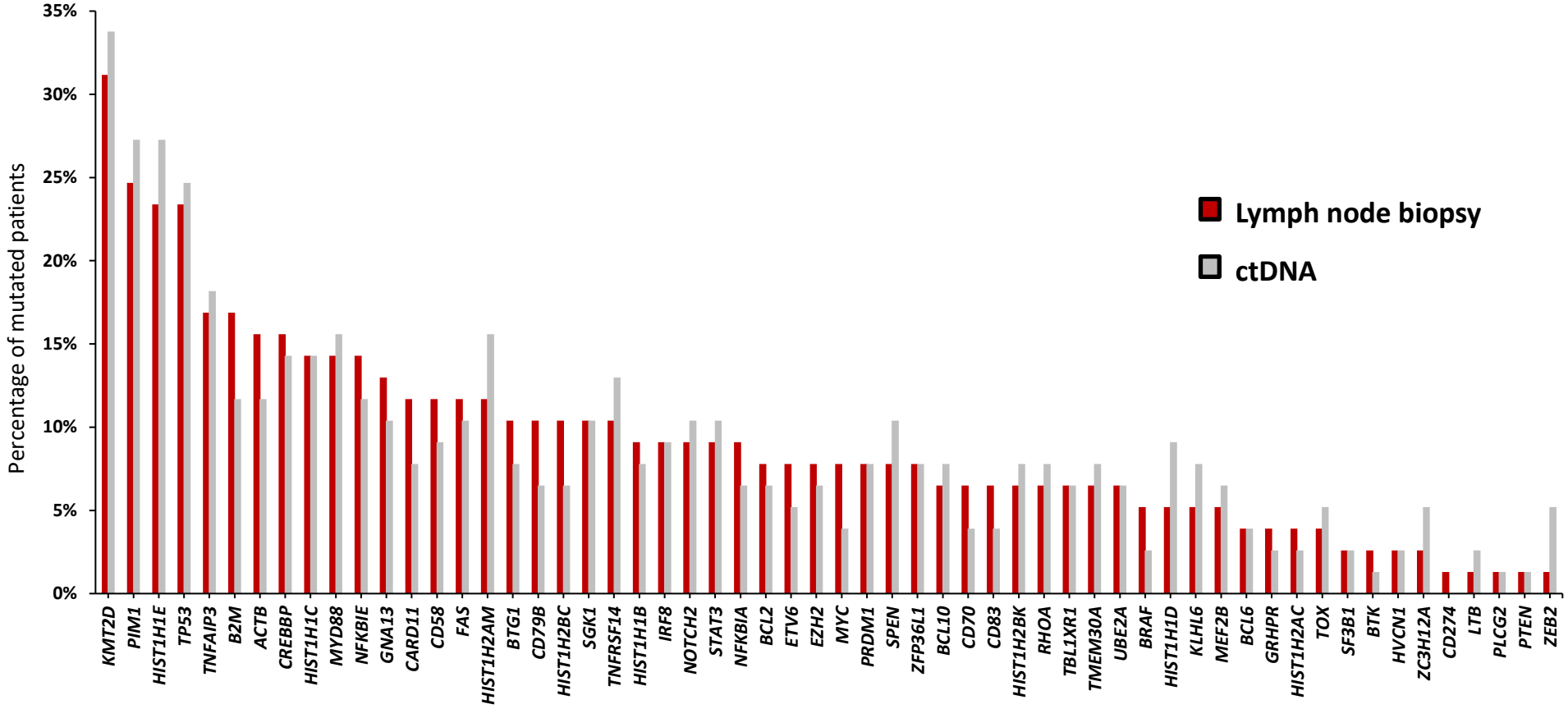


**Figure 3. Prevalence of mutations in tumor gDNA and ctDNA. A) The column chart represents the prevalence of genetic mutations found in tumor gDNA (N = 77), represented by red histograms. B) The column chart represents the prevalence of genetic mutations found in ctDNA (N = 77), represented by grey histograms. C) The column chart represents the prevalence of genetic mutations found in the lymph node compared to plasma ctDNA**

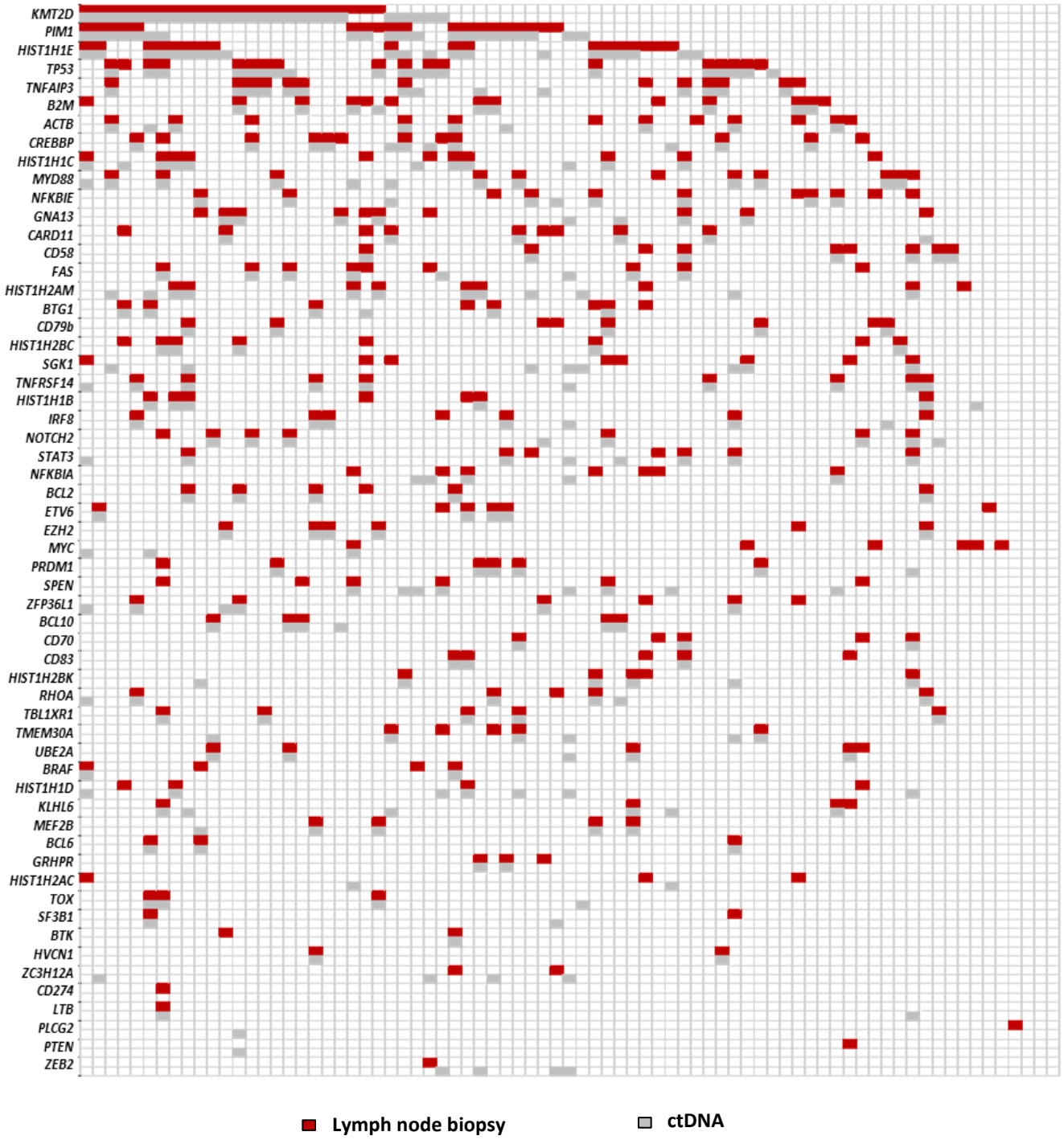


**Figure 4. Overview of the mutational profile identified in tumor gDNA from lymph node biopsy and ctDNA from plasma. Each column represents one patient, two rows represent one gene, first line represents tumor gDNA, and second line represents ctDNA. Mutations of tumor gDNA plotted in red, and mutations of ctDNA plotted in gray.**

## 4.3 ctDNA amount correlates with outcome

The amount of ctDNA in each DLBCL patient was estimated in terms of human genome equivalent (hGE) assuming a DNA content of 3.3 pg per cell. ctDNA level, expressed in hGE/mL of plasma, was calculated by multiplying the level of ctDNA, by the percentage of variant allele frequency obtained by sequencing. Higher levels of ctDNA (≥2.5 log10 hGE/mL) showed a significantly worse PFS ($p$ = 0.025) and OS ($p$ = 0.004) (Figure 5). The prognostic value of ctDNA ≥2.5 log10 hGE/mL maintained an independent association with PFS and OS when corrected with COO and clinical stage with a HR of 3.01 (95% CI 1.02-8.89, $p$= 0.046) and 5.52 (95% CI 1.19-25.59, $p$= 0.029), respectively (Table 2).

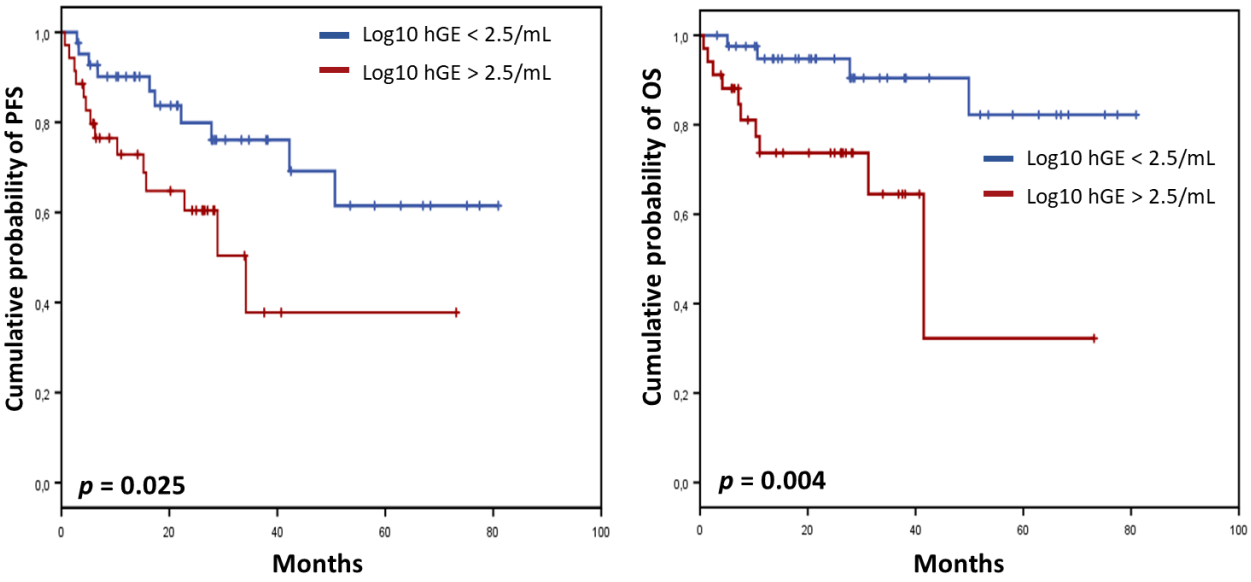


**Figure 5. Kaplan-Meier curves estimates of PFS and OS of Log10 hGE/mL in ctDNA. The red curves represent the ≥2.5 Log10 hGE/mL and the blue curves represent the < 2.5 Log10 hGE/mL. In the graph on the left the comparison has been made in terms of PFS and in the graph on the right in terms of OS.**

| | Progression free survival | | | Overall survival | | |
|---|---|---|---|---|---|---|
| **Characteristics** | **HR** | **95% CI** | ***P*** | **HR** | **95% CI** | ***P*** |
| **ctDNA ≥2.5 log10 hGE/mL** | 3.01 | 1.02-8.89 | 0.046 | 5.52 | 1.19-25.59 | 0.029 |
| **COO** | 2.29 | 0.66-6.63 | 0.645 | 2.23 | 0.45-11.02 | 0.645 |
| **Ann Arbor Stage** | 1.71 | 0.43-6.82 | 1.694 | 0.9 | 0.15-5.37 | 1.694 |

**Table 2. Multivariate analysis. COO, cell of origin; CI, confidence interval; HR, hazard ratio; P, P-value**

## 4.4 Clinical and prognostic impact of mutations

The clinical impact of the mutations detected in tumor gDNA from the LN biopsy and ctDNA was assessed in terms of PFS and OS.

*i) Prognostic factors identified in tumor gDNA*

*MYC* mutations were found in the tumor gDNA of 6 patients (7.79%) and were associated with a significantly shorter PFS (median = 5.3 months; $p = 0.021$) compared to wild type patients (Figure 6).

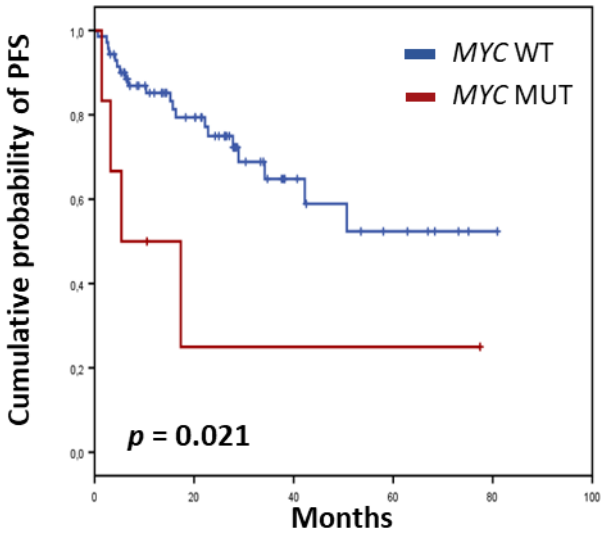


**Figure 6. Kaplan-Meier curves estimates of PFS of *MYC* mutated patients on tumor gDNA. The red corresponds to the mutated *MYC* patients, and the blue represents the wild type patients.**

*ii) Prognostic factors identified in ctDNA*

*GRHPR* mutations were found in the ctDNA of 2 patients (2.60%) and were associated with a significantly shorter PFS (median = 2.4 months; $p = 0.035$) compared to wild type patients (Figure 7).

*SGK1* mutations were found in the ctDNA of 8 patients (10.39%) and were associated with a significantly shorter PFS (median = 15.7 months; $p = 0.039$) compared to wild type patients (Figure 7).

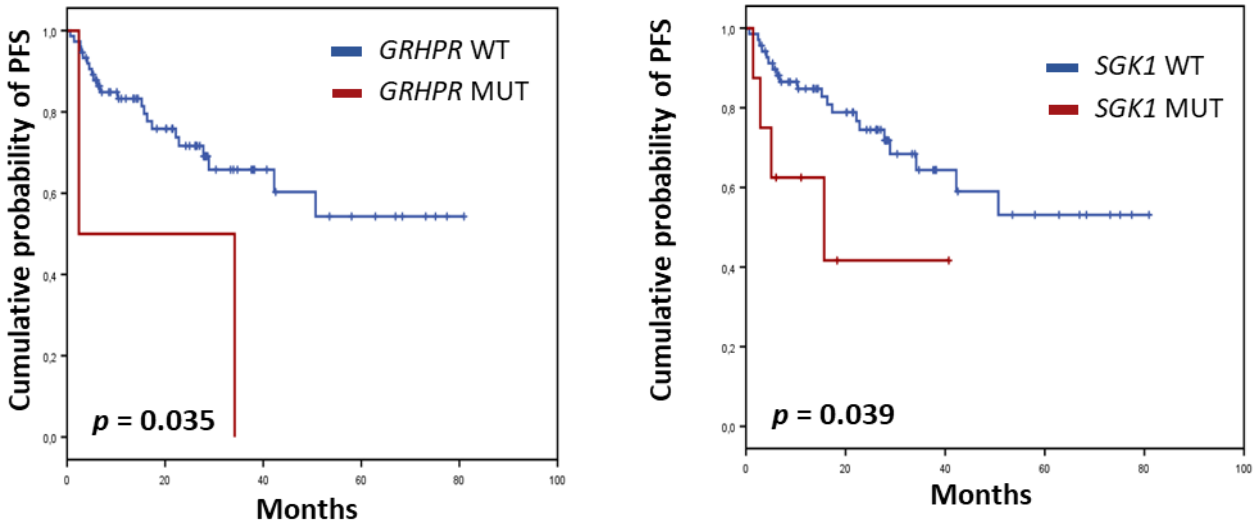


**Figure 7. Kaplan-Meier curves estimates of PFS of *GRHPR* and *SGK1* mutated patients on ctDNA. The red represents the mutated *GRHPR* and *SGK1* patients and the blue represents the wild type patients.**

## 4.5 Molecular clusters based on gene mutations in LN and plasma ctDNA compartments

Based on the mutational landscape identified in each compartment, DLBCL cases were analyzed with the LymphGen tool, that allows the cluster assignment in approximately 40-50% of DLBCLs. In our cohort, 46.5% (33/71) cases were assigned to a specific molecular cluster on the LN biopsy, among which 6/33 (18.18%) patients were classified in the BN2 subtype, 8/33 (24.24%) patients were classified in the EZB subtype, 9/33 (27.28%) patients were classified in the MCD subtype, 8/33 (24.24%) patients were classified in the ST2 subtype, 1/33 (3.03%) patient classified in BN2/ST2 subtype, and 1/33 (3.03%) patient classified in MCD/ST2 subtype. In the liquid biopsy, 40.3% (27/67) of cases were assigned to a specific molecular cluster, among which 5/27 (18.52%) patients were classified in the BN2 subtype, 7/27 (25.93%) patients were classified in the EZB subtype, 9/27 (33.33%) patients were classified in the MCD subtype, 5/27 (18.52%) patients were classified in the ST2 subtype, and 1/27 (3.70%) patient classified in BN2/ST2 subtype.

Interestingly, one case was classified as EZB on the LN biopsy and as MCD on the ctDNA. In all the other cases, if not unclassified, the cluster identified on the ctDNA reflected the cluster identified on the LN biopsy.

The combination of mutational data from LN and ctDNA improved DLBCL assignment to a specific cluster, thus classifying 48.7% (36/74) of cases. Among these, 6/36 (16.66%) patients were classified in the BN2 subtype, 8/36 (22.22%) patients were classified in the EZB subtype, 10/36 (27.78%) patients were classified in the MCD subtype, 10/36 (27.78%) patients were classified in the ST2 subtype, 1/36 (2.78%) patient classified in BN2/ST2 subtype, and 1/36 (2.78%) patient classified in MCD/ST2 subtype; these two patients were assigned to two different clusters and defined as “genetically composite”. From a clinical perspective, by combining mutational data from the LN and from ctDNA, patients belonging to the BN2 and ST2 clusters showed a favorable outcome with a 36-month PFS of 100% compared to 62.3% for patients belonging to the MCD or EZB clusters ($p = 0.040$) (Figure 8).

A

| ID | Cluster on LN | Cluster on ctDNA | Cluster combining LN and ctDNA |
|---|---|---|---|
| 20 | BN2 | Not classified | BN2 |
| 28 | BN2 | BN2 | BN2 |
| 52 | BN2 | BN2 | BN2 |
| 53 | BN2 | BN2 | BN2 |
| 61 | BN2 | BN2 | BN2 |
| 71 | BN2 | BN2 | BN2 |
| 68 | BN2/ST2 | BN2/ST2 | BN2/ST2 |
| 1 | EZB | EZB | EZB |
| 8 | EZB | EZB | EZB |
| 23 | EZB | EZB | EZB |
| 33 | EZB | EZB | EZB |
| 39 | EZB | EZB | EZB |
| 59 | EZB | EZB | EZB |
| 82 | EZB | MCD | EZB |
| 86 | EZB | EZB | EZB |
| 9 | MCD | MCD | MCD |
| 11 | MCD | MCD | MCD |
| 13 | MCD | MCD | MCD |
| 37 | MCD | Not classified | MCD |
| 38 | MCD | MCD | MCD |
| 58 | MCD | Not classified | MCD |
| 66 | MCD | MCD | MCD |
| 67 | MCD | MCD | MCD |
| 72 | MCD | MCD | MCD |
| 12 | Not classified | MCD | MCD |
| 41 | MCD/ST2 | Not classified | MCD/ST2 |
| 6 | ST2 | Not classified | ST2 |
| 17 | ST2 | ST2 | ST2 |
| 19 | ST2 | Not classified | ST2 |
| 55 | ST2 | ST2 | ST2 |
| 57 | ST2 | Not classified | ST2 |
| 64 | ST2 | Not classified | ST2 |
| 83 | ST2 | No_mut | ST2 |
| 84 | ST2 | ST2 | ST2 |
| 69 | No_mut | ST2 | ST2 |
| 22 | Not classified | ST2 | ST2 |

36 patients assigned to a specific moecular subtype among compartments

EZB ST2 MCD BN2 No mutation Not classified

B

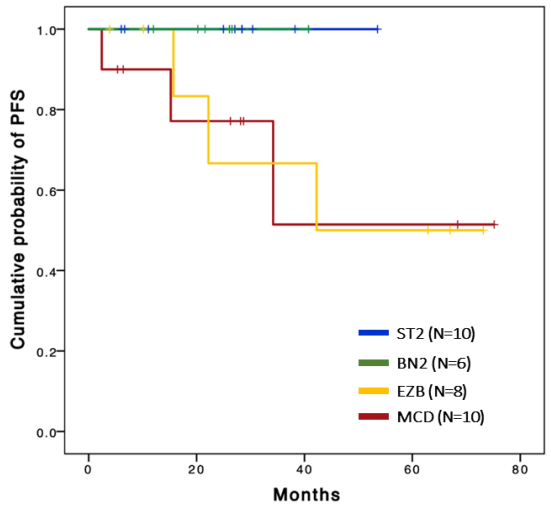


C

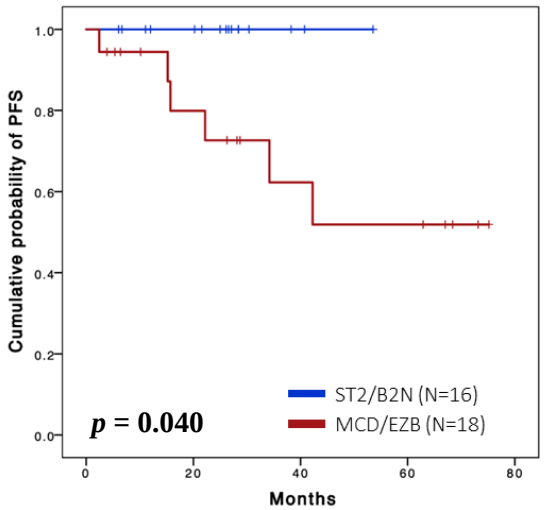


**Figure 8. A) Molecular clusters based on gene mutations; B and C) Clinical outcome of molecular clusters combining lymph node and ctDNA mutational data.**

# 5. DISCUSSION

In this study, we performed a mutational analysis of a real-life cohort of newly diagnosed DLBCL patients provided with paired lymph node biopsy tumor gDNA and plasma ctDNA. Results indicate that: *i)* the majority of the patients have at least one non-synonymous mutation in tumor gDNA and in plasma ctDNA, 92.2% and 87% respectively; *ii)* 25.38% of mutations identified in plasma ctDNA are not present in tumor gDNA, confirming the complementary role of liquid biopsy coupled with lymph node biopsy in DLBCL genotyping; *iii)* the most frequently mutated genes identified in both tumor gDNA and plasma ctDNA are *KMT2D*, *PIM1*, *HIST1H1E*, *TP53*, *TNFAIP3*; i*v) MYC* mutations, identified in the lymph node biopsy and *GRHPR* and *SGK1* mutations identified in plasma ctDNA samples, showed a significant association with a shorter PFS compared with wild type cases; *v)* by using the LymphGen tool, 33/71 (46.5%) cases were assigned to a specific molecular cluster on the lymph node biopsy, and 27/67 (40.3%) on the liquid biopsy; *vi)* the combination of mutational data from lymph node biopsy and from ctDNA improved DLBCL assignment to a specific cluster, thus classifying 48.7% (36/74) of cases.

Based upon the current international guidelines, a diagnosis of lymphoma is performed on a tissue biopsy (Swerdlow *et al.*, 2016). However, due to the high degree of molecular heterogeneity of DLBCL, mutational analysis of the tissue biopsy does not reflect the entire molecular heterogeneity of the disease. In this contest, liquid biopsy allows to collect ctDNA samples potentially deriving from all the different lymphoma sites and not only from one single anatomical compartment and can represent a useful approach to explore the entire mutational landscape of lymphoma (Rossi *et al.*, 2019). In our study, mutational analysis was performed on tumor gDNA and ctDNA samples for all 77 patients enrolled. Mutation analysis identified at least one somatic non-synonymous mutation in 92.2% (71/77) of patients in the lymph node biopsy, and in 87.0% (67/77) in the ctDNA. In total, 725 mutations have been identified, among which 362/725 (49.93%) mutations were shared in both compartments, 179/725 (24.69%) mutations were identified only in gDNA and 184/725 (25.38%) mutations only in ctDNA. These results reinforced the complementary role of liquid biopsy in disease genotyping with lymph node biopsy.

In a recent study, Kurtz *et al.* assessed ctDNA profiling by targeted high-throughput sequencing in DLBCL to explore the significance of pretreatment and dynamic ctDNA measurements for predicting outcomes in DLBCL. They showed that pretreatment ctDNA levels, with a threshold of 2.5 log hGE/mL, were prognostic and stratified patients outcomes

(Kurtz *et al.,* 2018*)*. In this cohort, our results validate the notion that higher levels of ctDNA (≥2.5 log hGE/mL) is significantly associated with worse PFS ($p = 0.025$) and OS ($p = 0.004$). In addition, the prognostic value of ctDNA ≥2.5 log10 hGE/mL maintained an independent association with PFS and OS when corrected with COO and clinical stage with a HR of 3.01 (95% CI 1.02-8.89, $p = 0.046$) and 5.52 (95% CI 1.19-25.59, $p = 0.029$) respectively.

Mutational analysis of different compartments, i.e., lymph node and plasma, allowed to identify mutations with potential clinical impact, that otherwise would have been missed with analysis of only one compartment. In particular, *GRHPR* ($p$=0.035) and *SGK1* ($p$=0.039) mutations identified only on the liquid biopsy, and *MYC* mutations identified only on the lymph node biopsy ($p$=0.021) showed a significant association with a shorter PFS.

Different approaches have been used to molecularly classify DLBCL. Initially GEP analyses on tissue biopsy have identified 3 subgroups of DLBCL, associated with a differential response to therapy, according to COO: ABC-DLBCL, GCB-DLBCL and unclassified (Alizadeh *et al.,* 2000; Rosenwald *et al.,* 2002; Wilson *et al.,* 2015). However, the COO classification does not fully consider the heterogeneous responses and outcomes, following therapy. In the recent years a series of large genomic and transcriptomic studies have been conducted to classify DLBCL in molecular cluster characterized by unique genetic features and therapeutic vulnerabilities (Chapuy *et al.,* 2018; Schmitz *et al.,* 2018, Wright *et al.,* 2020).

The first group identified in a cohort of primary DLBCLs five robust DLBCL subsets (C1-C5). The different genetic signatures also predict outcome independent of the clinical IPI and suggest new combination treatment strategies (Chapuy *et al.,* 2018). The second group identified four prominent genetic subtypes in DLBCL, termed MCD (based on the co-occurrence of *MYD88* L265P and *CD79B* mutations), BN2 (based on *BCL6* fusions and *NOTCH2* mutations), N1 (based on *NOTCH1* mutations), and EZB (based on *EZH2* mutations and *BCL2* translocations) (Schmitz *et al.*, 2018). In a subsequent study, Wright *et al*. devised an algorithm, termed LymphGen, to provide probabilistic classification of individual DLBCL patient into a genetic subtype, based on the presence specific genetic lesions (i.e., mutations, copy number variations (CNVs) or fusions).

In our study, based on the mutational landscape identified in each compartment, the LymphGen tool, as expected, allows the classification of each patient into a specific cluster in approximately 40-50% of DLBCL. More precisely, 46.5% (33/71) cases were assigned to a specific molecular cluster on the lymph node biopsy, and 40.3% (27/67) on the liquid biopsy. Interestingly, one case was classified as EZB on the lymph node biopsy and as MCD

on the ctDNA. In all the other cases, if not unclassified, the cluster identified on the ctDNA reflected the cluster identified on the lymph node biopsy. The combination of mutational data from lymph node and ctDNA improved DLBCL assignment to a specific cluster, thus classifying 48.7% (36/74) of cases. From a clinical perspective, by combining mutational data from the lymph node and from the ctDNA, patients belonging to the BN2 and ST2 clusters showed a favorable outcome with a 36-month PFS of 100% compared to 62.3% for patients belonging to the MCD or EZB clusters ($p = 0.040$).

Overall, the present study confirms the role of liquid biopsy as tool for disease genotyping and prognostic stratification in a real-life cohort of DLBCL patients. Moreover, the analysis of both ctDNA and lymph node biopsy provides complementary information for the molecular classification and prognostic stratification of newly diagnosed DLBCL patients. We are currently expanding the population cohort and we are starting the analysis of different time points during the course of therapy to validate the role of ctDNA for minimal residual disease monitoring.

# REFERENCES


Alizadeh AA, Eisen MB, Davis RE, Ma C, Lossos IS, Rosenwald A, Boldrick JC, Sabet H, Tran T, Yu X, Powell JI, Yang L, Marti GE, Moore T, Hudson J Jr, Lu L, Lewis DB, Tibshirani R, Sherlock G, Chan WC, Greiner TC, Weisenburger DD, Armitage JO, Warnke R, Levy R, Wilson W, Grever MR, Byrd JC, Botstein D, Brown PO, Staudt LM. Distinct types of diffuse large B-cell lymphoma identified by gene expression profiling. *Nature.* 2000; 403, 503–511.

Barrans SL, Evans PA, O'Connor SJ, Kendall SJ, Owen RG, Haynes AP, Morgan GJ, Jack AS. The t(14;18) is associated with germinal center-derived diffuse large B-cell lymphoma and is a strong predictor of outcome. *Clin Cancer Res*. 2003; 9(6):2133-2139.

Barrans S, Crouch S, Smith A, Crouch S, Smith A, Turner K, Owen R, Patmore R, Roman E, Jack A. Rearrangement of MYC is associated with poor prognosis in patients with diffuse large B-cell lymphoma treated in the era of rituximab. *J Clin Oncol*. 2010; 28(20):3360-3365.

Bereshchenko OR, Gu W, Dalla-Favera R. Acetylation inactivates the transcriptional repressor BCL6. *Nat Genet*. 2002; 32(4):606-613.

Boice M, Salloum D, Mourcin F, Sanghvi V, Amin R, Oricchio E, Jiang M, Mottok A, Denis-Lagache N, Ciriello G, Tam W, Teruya-Feldstein J, de Stanchina E, Chan WC, Malek SN, Ennishi D, Brentjens RJ, Gascoyne RD, Cogné M, Tarte K, Wendel HG. Loss of the HVEM Tumor Suppressor in Lymphoma and Restoration by Modified CAR-T Cells. *Cell*. 2016; 167(2):405-418.e13.

Boone DL, Turer EE, Lee EG, Ahmad RC, Wheeler MT, Tsui C, Hurley P, Chien M, Chai S, Hitotsumatsu O, McNally E, Pickart C, Ma A. The ubiquitin-modifying enzyme A20 is required for termination of Toll-like receptor responses. *Nat Immunol*. 2004; 5(10):1052-1060.

Brooks CL, Gu W. The impact of acetylation and deacetylation on the p53 pathway. *Protein Cell.* 2011; 2(6):456-462.

Burotto M, Berkovits A, Dunleavy K. Double hit lymphoma: from biology to therapeutic implications. *Expert Rev Hematol*. 2016; 9(7):669-678.

Carreras J, Lopez-Guillermo A, Kikuti YY, Itoh J, Masashi M, Ikoma H, Tomita S, Hiraiwa S, Hamoudi R, Rosenwald A, Leich E. High TNFRSF14 and low BTLA are associated with poor prognosis in Follicular Lymphoma and in Diffuse Large B-cell Lymphoma transformation. *Journal of clinical and experimental hematopathology*. 2019; 59(1):1-6.

Cattoretti G, Mandelbaum J, Lee N, Chaves AH, Mahler AM, Chadburn A, Dalla-Favera R, Pasqualucci L, MacLennan AJ. Targeted disruption of the S1P2 sphingosine 1-phosphate receptor gene leads to diffuse large B-cell lymphoma formation. *Cancer research*. 2009; 69(22):8686-92.

Challa-Malladi M, Lieu YK, Califano O, Holmes AB, Bhagat G, Murty VV, Dominguez-Sola D, Pasqualucci L, Dalla-Favera R. Combined genetic inactivation of β2-Microglobulin and CD58 reveals frequent escape from immune recognition in diffuse large B cell lymphoma. *Cancer Cell*. 2011; 20(6):728-40.

Chapuy B, Stewart C, Dunford AJ, Kim J, Kamburov A, Redd RA, Lawrence MS, Roemer MGM, Li AJ, Ziepert M, Staiger AM, Wala JA, Ducar MD, Leshchiner I, Rheinbay E, Taylor-Weiner A, Coughlin CA, Hess JM, Pedamallu CS, Livitz D, Rosebrock D, Rosenberg M, Tracy AA, Horn H, van Hummelen P, Feldman AL, Link BK, Novak AJ, Cerhan JR, Habermann TM, Siebert R, Rosenwald A, Thorner AR, Meyerson ML, Golub TR, Beroukhim R, Wulf GG, Ott G, Rodig SJ, Monti S, Neuberg DS, Loeffler M, Pfreundschuh M, Trümper L, Getz G, Shipp MA. Molecular subtypes of diffuse large B cell lymphoma are associated with distinct pathogenic mechanisms and outcomes. *Nat Med*. 2018; 24(5):679-690.

Cheson, BD, Pfistner B, Juweid ME, Gascoyne RD, Specht L, Horning SJ, Coiffier B, Fisher RI, Hagenbeek A, Zucca E, Rosen ST, Stroobants S, Lister TA, Hoppe RT, Dreyling M, Tobinai K, Vose JM, Connors JM, Federico M, Diehl V.; International Harmonization Project on Lymphoma. (2007) International harmonization project on L: r Revised response criteria for malignant lymphoma. *Journal of Clinical Oncology*. 2007; 25, :579–586.

Chiappella A, Tucci A, Castellino A, Pavone V, Baldi I, Carella AM, Orsucci L, Zanni M, Salvi F, Liberati AM, Gaidano G, Bottelli C, Rossini B, Perticone S, De Masi P, Ladetto M, Ciccone G, Palumbo A, Rossi G, Vitolo U; Fondazione Italiana Linfomi. Lenalidomide plus

cyclophosphamide, doxorubicin, vincristine, prednisone, and rituximab is safe and effective in untreated, elderly patients with diffuse large B-cell lymphoma: a phase I study by the Fondazione Italiana Linfomi. *Haematologica*. 2013; 98(11):1732-8.

Coiffier B, Sarkozy C. Diffuse large B-cell lymphoma: R-CHOP failure-what to do? *Hematology Am Soc Hematol Educ Program*. 2016; (1):366–378.

Compagno M, Lim WK, Grunn A, Nandula SV, Brahmachary M, Shen Q, Bertoni F, Ponzoni M, Scandurra M, Califano A, Bhagat G, Chadburn A, Dalla-Favera R, Pasqualucci L. Mutations of multiple genes cause deregulation of NF-kappaB in diffuse large B-cell lymphoma. *Nature*. 2009; 459(7247):717-21.

Conacci-Sorrell M, McFerrin L, Eisenman RN. An overview of MYC and its interactome. *Cold Spring Harb Perspect Med*. 2014; 4(1): a014357.

Czermin B, Melfi R, McCabe D, Seitz V, Imhof A, Pirrotta V. Drosophila enhancer of Zeste/ESC complexes have a histone H3 methyltransferase activity that marks chromosomal Polycomb sites. *Cell*. 2002; 111(2):185-196.

Dalla-Favera R, Pasqualucci L. Molecular Genetics of Lymphomas. In: Mauch PM, Armitage JO, Coiffier B, Dalla-Favera R, Harris NL, eds. Non-Hodgkin's Lymphoma. Philadelphia: *Lippincott Williams & Wilkins*. 2010; 825-843.

Davis RE, Ngo VN, Lenz G, Tolar P, Young RM, Romesser PB, Kohlhammer H, Lamy L, Zhao H, Yang Y, Xu W, Shaffer AL, Wright G, Xiao W, Powell J, Jiang JK, Thomas CJ, Rosenwald A, Ott G, Muller-Hermelink HK, Gascoyne RD, Connors JM, Johnson NA, Rimsza LM, Campo E, Jaffe ES, Wilson WH, Delabie J, Smeland EB, Fisher RI, Braziel RM, Tubbs RR, Cook JR, Weisenburger DD, Chan WC, Pierce SK, Staudt LM. Chronic active B-cell-receptor signaling in diffuse large B-cell lymphoma. *Nature*. 2010; 463(7277):88-92.

De Silva NS, Klein U. Dynamics of B cells in germinal centres. *Nature reviews. Immunology*. 2015; 15(3): 137–148.

Dierlamm J, Murga Penas EM, Bentink S, Wessendorf S, Berger H, Hummel M, Klapper W,

Lenze D, Rosenwald A, Haralambieva E, Ott G, Cogliatti SB, Möller P, Schwaenen C, Stein H, Löffler M, Spang R, Trümper L, Siebert R; Deutsche Krebshilfe Network Project "Molecular Mechanisms in Malignant Lymphomas". Gain of chromosome region 18q21 including the MALT1 gene is associated with the activated B-cell-like gene expression subtype and increased BCL2 gene dosage and protein expression in diffuse large B-cell lymphoma. *Haematologica*. 2008; 93:688–696.

Dominguez-Sola D, Kung J, Holmes AB, Wells VA, Mo T, Basso K, Dalla-Favera R. The FOXO1 transcription factor instructs the germinal center dark zone program. *Immunity*. 2015; 43(6):1064-1074.

Duan S, Cermak L, Pagan JK, Rossi M, Martinengo C, di Celle PF, Chapuy B, Shipp M, Chiarle R, Pagano M. FBXO11 targets BCL6 for degradation and is inactivated in diffuse large B-cell lymphomas. *Nature*. 2012; 481(7379):90-3.

Dubois S, Viailly PJ, Bohers E, Bertrand P, Ruminy P, Marchand V, Maingonnat C, Mareschal S, Picquenot JM, Penther D, Jais JP, Tesson B, Peyrouze P, Figeac M, Desmots F, Fest T, Haioun C, Lamy T, Copie-Bergman C, Fabiani B, Delarue R, Peyrade F, André M, Ketterer N, Leroy K, Salles G, Molina TJ, Tilly H, Jardin F. Biological and clinical relevance of associated genomic alterations in MYD88 L265P and non-L265P-mutated diffuse large B-cell lymphoma: analysis of 361 cases. *Clin. Cancer Res*. 2017; 23:2232–2244.

Dunleavy K, Wilson WH. Appropriate management of molecular subtypes of diffuse large B-cell lymphoma. *Oncology (Williston Park)*. 2014; 28(4):326-334.

Ennishi D, Mottok A, Ben-Neriah S, Shulha HP, Farinha P, Chan FC, Meissner B, Boyle M, Hother C, Kridel R, Lai D, Saberi S, Bashashati A, Shah SP, Morin RD, Marra MA, Savage KJ, Sehn LH, Steidl C, Connors JM, Gascoyne RD, Scott DW. Genetic profiling of MYC and BCL2 in diffuse large B-cell lymphoma determines cell-of-origin-specific clinical impact. *Blood*. 2017; 129(20):2760-2770.

Fleischhacker M, Schmidt B. Circulating nucleic acids (CNAs) and cancer--a survey. *Biochim Biophys Acta*. 2007; 1775(1):181–232.

Goodman RH, Smolik S. CBP/p300 in cell growth, transformation, and development. *Genes Dev*. 2000; 14(13):1553-1577.

Green TM, Young KH, Visco C, Xu-Monette ZY, Orazi A, Go RS, Nielsen O, Gadeberg OV, Mourits-Andersen T, Frederiksen M, Pedersen LM, Møller MB. Immunohistochemical double-hit score is a strong predictor of outcome in patients with diffuse large B-cell lymphoma treated with rituximab plus cyclophosphamide, doxorubicin, vincristine, and prednisone. *J Clin Oncol*. 2012; 30(28): 3460–346–-7.

Hans CP, Weisenburger DD, Greiner TC, Gascoyne RD, Delabie J, Ott G, Müller-Hermelink HK, Campo E, Braziel RM, Jaffe ES, Pan Z, Farinha P, Smith LM, Falini B, Banham AH, Rosenwald A, Staudt LM, Connors JM, Armitage JO, Chan WC. Confirmation of the molecular classification of diffuse large B-cell lymphoma by immunohistochemistry using a tissue microarray. *Blood*. 2004; 103(1):275-82.

Hohaus S, Giachelia M, Massini G, Mansueto G, Vannata B, Bozzoli V, Criscuolo M, D'Alò F, Martini M, Larocca LM, Voso MT, Leone G. Cell-free circulating DNA in Hodgkin's and non-Hodgkin's lymphomas. *Ann Oncol*. 2009; 20(8):1408–13.

Ichikawa A, Kinoshita T, Watanabe T, Kato H, Nagai H, Tsushita K, Saito H, Hotta T. Mutations of the p53 gene as a prognostic factor in aggressive B-cell lymphoma. *N Engl J Med*. 1997; 337(8):529-34.

Iqbal J, Greiner TC, Patel K, Dave BJ, Smith L, Ji J, Wright G, Sanger WG, Pickering DL, Jain S, Horsman DE, Shen Y, Fu K, Weisenburger DD, Hans CP, Campo E, Gascoyne RD, Rosenwald A, Jaffe ES, Delabie J, Rimsza L, Ott G, Müller-Hermelink HK, Connors JM, Vose JM, McKeithan T, Staudt LM, Chan WC; Leukemia/Lymphoma Molecular Profiling Project. Distinctive patterns of BCL6 molecular alterations and their functional consequences in different subgroups of diffuse large B-cell lymphoma. *Leukemia.* 2007; 21(11):2332-43.

Iqbal J, Sanger WG, Horsman DE, Rosenwald A, Pickering DL, Dave B, Dave S, Xiao L, Cao K, Zhu Q, Sherman S, Hans CP, Weisenburger DD, Greiner TC, Gascoyne RD, Ott G, Müller-Hermelink HK, Delabie J, Braziel RM, Jaffe ES, Campo E, Lynch JC, Connors JM, Vose JM, Armitage JO, Grogan TM, Staudt LM, Chan WC. BCL2 translocation defines a unique tumor

subset within the germinal center B-cell-like diffuse large B-cell lymphoma. *Am J Pathol*. 2004; 165(1):159-66.

Jahr S, Hentze H, Englisch S, Hardt D, Fackelmayer FO, Hesch RD, Knippers R. DNA fragments in the blood plasma of cancer patients: quantitations and evidence for their origin from apoptotic and necrotic cells. *Cancer Res*. 2001; 61(4):1659–65.

Karube K, Campo E. MYC alterations in diffuse large B-cell lymphomas. *Semin Hematol*. 2015; 52(2):97-106.

Karube K, Enjuanes A, Dlouhy I, Jares P, Martin-Garcia D, Nadeu F, Ordóñez GR, Rovira J, Clot G, Royo C, Navarro A, Gonzalez-Farre B, Vaghefi A, Castellano G, Rubio-Perez C, Tamborero D, Briones J, Salar A, Sancho JM, Mercadal S, Gonzalez-Barca E, Escoda L, Miyoshi H, Ohshima K, Miyawaki K, Kato K, Akashi K, Mozos A, Colomo L, Alcoceba M, Valera A, Carrió A, Costa D, Lopez-Bigas N, Schmitz R, Staudt LM, Salaverria I, López-Guillermo A, Campo E. Integrating genomic alterations in diffuse large B-cell lymphoma identifies new relevant pathways and potential therapeutic targets. *Leukemia*. 2018; 32(3):675-684.

Kato M, Sanada M, Kato I, Sato Y, Takita J, Takeuchi K, Niwa A, Chen Y, Nakazaki K, Nomoto J, Asakura Y, Muto S, Tamura A, Iio M, Akatsuka Y, Hayashi Y, Mori H, Igarashi T, Kurokawa M, Chiba S, Mori S, Ishikawa Y, Okamoto K, Tobinai K, Nakagama H, Nakahata T, Yoshino T, Kobayashi Y, Ogawa S. Frequent inactivation of A20 in B-cell lymphomas. *Nature*. 2009; 459(7247):712-716.

Kerbauy FR, Colleoni GW, Saad ST, Regis Silva MR, Correa Alves A, Aguiar KC, Albuquerque DM, Kobarg J, Seixas MT, Kerbauy J. Detection and possible prognostic relevance of p53 gene mutations in diffuse large B-cell lymphoma. An analysis of 51 cases and review of the literature. *Leuk Lymphoma*. 2004; 45(10):2071-8.

Knies N, Alankus B, Weilemann A, Tzankov A, Brunner K, Ruff T, Kremer M, Keller UB, Lenz G, Ruland J. Lymphomagenic CARD11/BCL10/MALT1 signaling drives malignant B-cell proliferation via cooperative NF-κB and JNK activation. *Proc Natl Acad Sci* U S A. 2015; 112(52):E7230-8.

Kurtz DM, Green MR, Bratman SV, Scherer F, Liu CL, Kunder CA, Takahashi K, Glover C, Keane C, Kihira S, Visser B, Callahan J, Kong KA, Faham M, Corbelli KS, Miklos D, Advani RH, Levy R, Hicks RJ, Hertzberg M, Ohgami RS, Gandhi MK, Diehn M, Alizadeh AA. Noninvasive monitoring of diffuse large B-cell lymphoma by immunoglobulin high-throughput sequencing. *Blood*. 2015; 125(24):3679-87.

Kurtz DM, Scherer F, Jin MC, Soo J, Craig AFM, Esfahani MS, Chabon JJ, Stehr H, Liu CL, Tibshirani R, Maeda LS, Gupta NK, Khodadoust MS, Advani RH, Levy R, Newman AM, Dührsen U, Hüttmann A, Meignan M, Casasnovas RO, Westin JR, Roschewski M, Wilson WH, Gaidano G, Rossi D, Diehn M, Alizadeh AA. Circulating Tumor DNA Measurements As Early Outcome Predictors in Diffuse Large B-Cell Lymphoma. *J Clin Oncol*. 2018 1;36(28):2845-2853.

Kwak JY. Treatment of diffuse large B cell lymphoma. *Korean J Intern Med*. 2012; 27(4):369–377.

Lam LT, Wright G, Davis RE, Lenz G, Farinha P, Dang L, Chan JW, Rosenwald A, Gascoyne RD, Staudt LM. Cooperative signaling through the signal transducer and activator of transcription 3 and nuclear factor-{kappa}B pathways in subtypes of diffuse large B-cell lymphoma. *Blood*. 2008; 111(7):3701-13.

Lenz G, Davis RE, Ngo VN, Lam L, George TC, Wright GW, Dave SS, Zhao H, Xu W, Rosenwald A, Ott G, Muller-Hermelink HK, Gascoyne RD, Connors JM, Rimsza LM, Campo E, Jaffe ES, Delabie J, Smeland EB, Fisher RI, Chan WC, Staudt LM. Oncogenic CARD11 mutations in human diffuse large B cell lymphoma. *Science*. 2008; 319(5870):1676-1679.

Li S, Young KH, Medeiros LJ. Diffuse large B-cell lymphoma. *Pathology*. 2018; 50(1):74-87.

Liu Y, Barta SK. Diffuse large B-cell lymphoma: 2019 update on diagnosis, risk stratification, and treatment. *American journal of hematology*. 2019; 94(5):604-16.

McCabe MT, Ott HM, Ganji G, Korenchuk S, Thompson C, Van Aller GS, Liu Y, Graves AP, Diaz E, LaFrance LV, Mellinger M. EZH2 inhibition as a therapeutic strategy for lymphoma

with EZH2-activating mutations. *Nature*. 2012; 492(7427):108-12.

Mesin L, Ersching J, Victora GD. Germinal Center B Cell Dynamics. *Immunity*. 2016; 45(3):471–482.

Miller SA, Dykes DD, Polesky HF. A simple salting out procedure for extracting DNA from human nucleated cells. *Nucleic Acids Res*. 1988; 16(3):1215.

Moia R, Favini C, Rasi S, Deambrogi C, Ferri V, Schipani M, Sagiraju S, Mahmoud AM, Kodipad AA, Adhinaveni R, Patriarca A. Liquid biopsy in lymphomas: A potential tool for refining diagnosis and disease monitoring. *Journal of Cancer Metastasis and Treatment*. 2019; 4-5.

Monti S, Chapuy B, Takeyama K, Rodig SJ, Hao Y, Yeda KT, Inguilizian H, Mermel C, Currie T, Dogan A, Kutok JL, Beroukhim R, Neuberg D, Habermann TM, Getz G, Kung AL, Golub TR, Shipp MA. Integrative analysis reveals an outcome-associated and targetable pattern of p53 and cell cycle deregulation in diffuse large B cell lymphoma. *Cancer Cell*. 2012; 22(3):359-72.

Morin RD, Johnson NA, Severson TM, Mungall AJ, An J, Goya R, Paul JE, Boyle M, Woolcock BW, Kuchenbauer F, Yap D, Humphries RK, Griffith OL, Shah S, Zhu H, Kimbara M, Shashkin P, Charlot JF, Tcherpakov M, Corbett R, Tam A, Varhol R, Smailus D, Moksa M, Zhao Y, Delaney A, Qian H, Birol I, Schein J, Moore R, Holt R, Horsman DE, Connors JM, Jones S, Aparicio S, Hirst M, Gascoyne RD, Marra MA. Somatic mutations altering EZH2 (Tyr641) in follicular and diffuse large B-cell lymphomas of germinal-center origin. *Nat Genet*. 2010; 42(2):181-5.

Morin RD, Mendez-Lago M, Mungall AJ, Goya R, Mungall KL, Corbett RD, Johnson NA, Severson TM, Chiu R, Field M, Jackman S, Krzywinski M, Scott DW, Trinh DL, Tamura-Wells J, Li S, Firme MR, Rogic S, Griffith M, Chan S, Yakovenko O, Meyer IM, Zhao EY, Smailus D, Moksa M, Chittaranjan S, Rimsza L, Brooks-Wilson A, Spinelli JJ, Ben-Neriah S, Meissner B, Woolcock B, Boyle M, McDonald H, Tam A, Zhao Y, Delaney A, Zeng T, Tse K, Butterfield Y, Birol I, Holt R, Schein J, Horsman DE, Moore R, Jones SJ, Connors JM, Hirst M, Gascoyne RD, Marra MA. Frequent mutation of histone-modifying genes in non-Hodgkin

lymphoma. *Nature.* 2011; 476(7360):298-303.

Muppidi JR, Schmitz R, Green JA, Xiao W, Larsen AB, Braun SE, An J, Xu Y, Rosenwald A, Ott G, Gascoyne RD. Loss of signaling via Gα13 in germinal centre B-cell-derived lymphoma. *Nature*. 2014; 516(7530):254-8.

Ngo VN, Young RM, Schmitz R, Jhavar S, Xiao W, Lim KH, Kohlhammer H, Xu W, Yang Y, Zhao H, Shaffer AL, Romesser P, Wright G, Powell J, Rosenwald A, Muller-Hermelink HK, Ott G, Gascoyne RD, Connors JM, Rimsza LM, Campo E, Jaffe ES, Delabie J, Smeland EB, Fisher RI, Braziel RM, Tubbs RR, Cook JR, Weisenburger DD, Chan WC, Staudt LM. Oncogenically active MYD88 mutations in human lymphoma. *Nature*. 2011; 470(7332):115-9.

Pasqualucci L, Dalla-Favera R. Genetics of diffuse large B-cell lymphoma. *Blood*. 2018; 131(21):2307-2319.

Pasqualucci L, Dominguez-Sola D, Chiarenza A, Fabbri G, Grunn A, Trifonov V, Kasper LH, Lerach S, Tang H, Ma J, Rossi D, Chadburn A, Murty VV, Mullighan CG, Gaidano G, Rabadan R, Brindle PK, Dalla-Favera R. Inactivating mutations of acetyltransferase genes in B-cell lymphoma. *Nature*. 2011; 471(7337):189-95.

Pasqualucci L, Migliazza A, Basso K, Houldsworth J, Chaganti RS, Dalla-Favera R. Mutations of the BCL6 proto-oncogene disrupt its negative autoregulation in diffuse large B-cell lymphoma. *Blood*. 2003; 101(8):2914-2923.

Pasqualucci L, Migliazza A, Fracchiolla N, William C, Neri A, Baldini L, Chaganti RS, Klein U, Küppers R, Rajewsky K, Dalla-Favera R. BCL-6 mutations in normal germinal center B cells: evidence of somatic hypermutation acting outside Ig loci. *Proc Natl Acad Sci* U S A. 1998; 95(20):11816-21.

Pasqualucci L, Trifonov V, Fabbri G, Ma J, Rossi D, Chiarenza A, Wells VA, Grunn A, Messina M, Elliot O, Chan J, Bhagat G, Chadburn A, Gaidano G, Mullighan CG, Rabadan R, Dalla-Favera R. Analysis of the coding genome of diffuse large B-cell lymphoma. *Nat Genet*. 2011; 43(9):830-7.

Pitzalis C, Jones GW, Bombardieri M, Jones SA. Ectopic lymphoid-like structures in infection, cancer, and autoimmunity. *Nat Rev Immunol*. 2014; 14(7):447-62.

Rhyasen GW, Starczynowski DT. IRAK signaling in cancer. *Br J Cancer*. 2015; 112(2):232–237.

Roschewski M, Dunleavy K, Pittaluga S, Moorhead M, Pepin F, Kong K, Shovlin M, Jaffe ES, Staudt LM, Lai C, Steinberg SM, Chen CC, Zheng J, Willis TD, Faham M, Wilson WH. Circulating tumor DNA and CT monitoring in patients with untreated diffuse large B-cell lymphoma: a correlative biomarker study. *Lancet Oncol.* 2015; 16(5):541-9.

Roschewski M, Staudt LM, Wilson WH. Dynamic monitoring of circulating tumor DNA in non-Hodgkin lymphoma. *Blood*. 2016; 127(25):3127-3132.

Rosenthal, A, Younes, A. High grade B-cell lymphoma with rearrangements of MYC and BCL2 and/or BCL6: double hit and triple hit lymphomas and double expressing lymphoma. *Blood Rev*. 2017; 31: 37–42.

Rosenwald A, Wright G, Chan WC, Connors JM, Campo E, Fisher RI, Gascoyne RD, Muller-Hermelink HK, Smeland EB, Giltnane JM, Hurt EM, Zhao H, Averett L, Yang L, Wilson WH, Jaffe ES, Simon R, Klausner RD, Powell J, Duffey PL, Longo DL, Greiner TC, Weisenburger DD, Sanger WG, Dave BJ, Lynch JC, Vose J, Armitage JO, Montserrat E, López-Guillermo A, Grogan TM, Miller TP, LeBlanc M, Ott G, Kvaloy S, Delabie J, Holte H, Krajci P, Stokke T, Staudt LM for the Lymphoma/Leukemia Molecular Profiling Project. The use of molecular profiling to predict survival after chemotherapy for diffuse large-B-cell lymphoma. *N Engl J Med.* 2002; 346(25):1937-1947.

Rossi D, Diop F, Spaccarotella E, Monti S, Zanni M, Rasi S, Deambrogi C, Spina V, Bruscaggin A, Favini C, Serra R. Diffuse large B-cell lymphoma genotyping on the liquid biopsy. *Blood, The Journal of the American Society of Hematology*. 2017; 129(14):1947-57.

Rushton C, Alcaide M, Cheung M, Thomas N, Arthur S, Michaud N, Daigle S, Davidson J, Bushell K, Yu S, Jain M, Shepherd L, Crump M, Mann K, Kuruvilla J, Assouline S, Johnson

N, Scott DW, Morin RD. Identifying Mutations Enriched in Relapsed-Refractory Dlbcl to Derive Genetic Factors Underlying Treatment Resistance. *Hematol. Oncol*. 2019; 37, :35–36.

Saito M, Novak U, Piovan E, Basso K, Sumazin P, Schneider C, Crespo M, Shen Q, Bhagat G, Califano A, Chadburn A, Pasqualucci L, Dalla-Favera R. BCL6 suppression of BCL2 via Miz1 and its disruption in diffuse large B cell lymphoma. *Proc Natl Acad Sci* U S A. 2009; 106(27):11294-9.

Schmitz R, Wright GW, Huang DW, Johnson CA, Phelan JD, Wang JQ, Roulland S, Kasbekar M, Young RM, Shaffer AL, Hodson DJ, Xiao W, Yu X, Yang Y, Zhao H, Xu W, Liu X, Zhou B, Du W, Chan WC, Jaffe ES, Gascoyne RD, Connors JM, Campo E, Lopez-Guillermo A, Rosenwald A, Ott G, Delabie J, Rimsza LM, Tay Kuang Wei K, Zelenetz AD, Leonard JP, Bartlett NL, Tran B, Shetty J, Zhao Y, Soppet DR, Pittaluga S, Wilson WH, Staudt LM. Genetics and Pathogenesis of Diffuse Large B-Cell Lymphoma. *New England Journal of Medicine*. 2018; 378(15):1396-1407.

Schneider C, Kon N, Amadori L, Shen Q, Schwartz FH, Tischler B, Bossennec M, Dominguez-Sola D, Bhagat G, Gu W, Basso K, Dalla-Favera R. FBXO11 inactivation leads to abnormal germinal-center formation and lymphoproliferative disease. *Blood*. 2016; 128(5):660-666.

Scott DW, Mottok A, Ennishi D, Wright GW, Farinha P, Ben-Neriah S, Kridel R, Barry GS, Hother C, Abrisqueta P, Boyle M, Meissner B, Telenius A, Savage KJ, Sehn LH, Slack GW, Steidl C, Staudt LM, Connors JM, Rimsza LM, Gascoyne RD. Prognostic Significance of Diffuse Large B-Cell Lymphoma Cell of Origin Determined by Digital Gene Expression in Formalin-Fixed Paraffin-Embedded Tissue Biopsies. *J Clin Oncol*. 2015; 33(26):2848-56.

Shaffer AL 3rd, Young RM, Staudt LM. Pathogenesis of Human B Cell Lymphomas. *Annual Review of Immunology*. 2012; 30:1, 565-610.

Shen HM, Peters A, Baron B, Zhu X, Storb U. Mutation of BCL-6 gene in normal B cells by the process of somatic hypermutation of Ig genes. *Science*. 1998; 280(5370):1750-1752.

Shilatifard A. The COMPASS family of histone H3K4 methylases: mechanisms of regulation in development and disease pathogenesis. *Annu Rev Biochem*. 2012; 81:65-95.

Sneeringer CJ, Scott MP, Kuntz KW, Knutson SK, Pollock RM, Richon VM, Copeland RA. Coordinated activities of wild-type plus mutant EZH2 drive tumor-associated hypertrimethylation of lysine 27 on histone H3 (H3K27) in human B-cell lymphomas. *Proc Natl Acad Sci* U S A. 2010; 107(49):20980-5.

Spina V, Rossi D., Liquid biopsy in tissue-born lymphomas. *Swiss Med Wikly*. 2019; 149:14709.

Stebegg M, Kumar SD, Silva-Cayetano A, Fonseca VR, Linterman MA, Graca L. Regulation of the germinal center response. *Frontiers in immunology*. 2018; 9:2469.

Steinberg MW, Cheung TC, Ware CF. The signaling networks of the herpesvirus entry mediator (TNFRSF14) in immune regulation. *Immunol Rev*. 2011; 244(1):169-187.

Swerdlow SH, Campo E, Pileri SA, Harris NL, Stein H, Siebert R, Advani R, Ghielmini M, Salles GA, Zelenetz AD, Jaffe ES. The 2016 revision of the World Health Organization classification of lymphoid neoplasms. *Blood*. 2016; 127(20):2375-90.

Teras LR, DeSantis CE, Cerhan JR, MD, Morton LM, Jemal A, Flowers CR. MS6 2016 US Lymphoid Malignancy Statistics by World Health Organization Subtypes. *CA Cancer J Clin.* 2016; 66:443–459.

Thieblemont C, Briere J, Mounier N, Voelker HU, Cuccuini W, Hirchaud E, Rosenwald A, Jack A, Sundstrom C, Cogliatti S, Trougouboff P, Boudova L, Ysebaert L, Soulier J, Chevalier C, Bron D, Schmitz N, Gaulard P, Houlgatte R, Gisselbrecht C. The germinal center/activated B-cell subclassification has a prognostic impact for response to salvage therapy in relapsed/refractory diffuse large B-cell lymphoma: a bio-CORAL study. *J Clin Oncol.* 2011; 29(31):4079-87.

Thome M. CARMA1, BCL-10 and MALT1 in lymphocyte development and activation. *Nat Rev Immunol*. 2004; 4(5):348-359.

Tilly H, Gomes da Silva M, Vitolo U, Jack A, Meignan M, Lopez-Guillermo A, Walewski

J, André M, Johnson PW, Pfreundschuh M, Ladetto M; ESMO Guidelines Committee. Diffuse large B-cell lymphoma (DLBCL): ESMO Clinical Practice Guidelines for diagnosis, treatment and follow-up. *Ann Oncol*. 2015; 26 Suppl (5): v116-25.

Trinh DL, Scott DW, Morin RD, Mendez-Lago M, An J, Jones SJ, Mungall AJ, Zhao Y, Schein J, Steidl C, Connors JM, Gascoyne RD, Marra MA. Analysis of FOXO1 mutations in diffuse large B-cell lymphoma. *Blood*. 2013; 121(18):3666-74.

Wang X, Li Z, Naganuma A, Ye BH. Negative autoregulation of BCL-6 is bypassed by genetic alterations in diffuse large B cell lymphomas. *Proc Natl Acad Sci U S A.* 2002; 99(23):15018-23.

Wilson WH, Young RM, Schmitz R, Yang Y, Pittaluga S, Wright G, Lih CJ, Williams PM, Shaffer AL, Gerecitano J, de Vos S, Goy A, Kenkre VP, Barr PM, Blum KA, Shustov A, Advani R, Fowler NH, Vose JM, Elstrom RL, Habermann TM, Barrientos JC, McGreivy J, Fardis M, Chang BY, Clow F, Munneke B, Moussa D, Beaupre DM, Staudt LM. Targeting B cell receptor signaling with ibrutinib in diffuse large B cell lymphoma. *Nat Med*. 2015; 21, 922–926.

Wright GW, Phelan JD, Coulibaly ZA, Roulland S, Young RM, Wang JQ, Schmitz R, Morin RD, Tang J, Jiang A, Bagaev A. A probabilistic classification tool for genetic subtypes of diffuse large B cell lymphoma with therapeutic implications. *Cancer Cell*. 2020; 37(4):551-68.

Xu-Monette ZY, Wu L, Visco C, Tai YC, Tzankov A, Liu WM, Montes-Moreno S, Dybkaer K, Chiu A, Orazi A, Zu Y, Bhagat G, Richards KL, Hsi ED, Zhao XF, Choi WW, Zhao X, van Krieken JH, Huang Q, Huh J, Ai W, Ponzoni M, Ferreri AJ, Zhou F, Kahl BS, Winter JN, Xu W, Li J, Go RS, Li Y, Piris MA, Møller MB, Miranda RN, Abruzzo LV, Medeiros LJ, Young KH. Mutational profile and prognostic significance of TP53 in diffuse large B-cell lymphoma patients treated with R-CHOP: report from an International DLBCL Rituximab-CHOP Consortium Program Study. *Blood*. 2012; 120(19):3986-96.

Ye BH, Chaganti S, Chang CC, Niu H, Corradini P, Chaganti RS, Dalla-Favera R. Chromosomal translocations cause deregulated BCL6 expression by promoter substitution in B cell lymphoma. *EMBO J.* 1995; 14(24):6209-6217.

Ying CY, Dominguez-Sola D, Fabi M, Lorenz IC, Hussein S, Bansal M, Califano A, Pasqualucci L, Basso K, Dalla-Favera R. MEF2B mutations lead to deregulated expression of the oncogene BCL6 in diffuse large B cell lymphoma. *Nat Immunol*. 2013; 14(10):1084-92.

Young KH, Weisenburger DD, Dave BJ, Smith L, Sanger W, Iqbal J, Campo E, Delabie J, Gascoyne RD, Ott G, Rimsza L, Müller-Hermelink HK, Jaffe ES, Rosenwald A, Staudt LM, Chan WC, Greiner TC. Mutations in the DNA-binding codons of TP53, which are associated with decreased expression of TRAILreceptor-2, predict for poor survival in diffuse large B-cell lymphoma. *Blood*. 2007; 110(13):4396-405.

Zhang J, Dominguez-Sola D, Hussein S, Lee JE, Holmes AB, Bansal M, Vlasevska S, Mo T, Tang H, Basso K, Ge K, Dalla-Favera R, Pasqualucci L. Disruption of KMT2D perturbs germinal center B cell development and promotes lymphomagenesis. *Nat Med*. 2015; 21(10):1190-8.